Widening the landscape of transcriptional regulation of green algal photoprotection

Authors

Marius Arend[1,2,3†], Yizhong Yuan[4†], M. Águila Ruiz-Sola[4‡], Nooshin Omranian[1,2,3], Zoran Nikoloski[1,23*], Dimitris Petroutsos[4 *]

Affiliations

[1]Bioinformatics Group, Institute of Biochemistry and Biology, University of Potsdam, 14476 Potsdam, Germany

[2]Systems Biology and Mathematical Modeling Group, Max-Planck-Institute of Molecular Plant Physiology, 14476 Potsdam, Germany

[3]Bioinformatics and Mathematical Modeling Department, Center of Plant Systems Biology and Biotechnology, 4000 Plovdiv, Bulgaria

[4]University of Grenoble Alpes, CNRS, CEA, INRAE, IRIG-LPCV, 38000 Grenoble, France

[†] These authors contributed equally to this work

[‡] Current address: Instituto de Bioquímica Vegetal y Fotosíntesis, Universidad de Sevilla-CSIC, 41092, Sevilla, SPAIN

[*]**Corresponding Authors**: nikoloski@mpimp-golm.mpg.de (Z.N.), dimitrios.petroutsos@cnrs.fr (D.P.)

Abstract

Availability of light and CO_2, substrates of microalgae photosynthesis, is frequently far from optimal. Microalgae activate photoprotection under strong light, to prevent oxidative damage, and the CO_2 Concentrating Mechanism (CCM) under low CO_2, to raise intracellular CO_2 levels. The two processes are interconnected; yet, the underlying transcriptional regulators remain largely unknown. Employing a large transcriptomics data compendium of *Chlamydomonas reinhardtii's* responses to different light and carbon supply, we reconstructed a consensus genome-scale gene regulatory network from complementary inference approaches and used it to elucidate transcriptional regulators of photoprotection. We showed that the CCM regulator LCR1 also controls photoprotection, and that QER7, a Squamosa Binding Protein, suppresses photoprotection- and CCM-gene expression under the control of the blue light photoreceptor Phototropin. By demonstrating the existence of regulatory hubs that channel light- and CO_2-mediated signals into a common response, our study provides an accessible resource to dissect gene expression regulation in this microalga.

37 **Introduction**

38 Photosynthetic microalgae convert light into chemical energy in the form of ATP and NADPH to fuel the CO_2
39 fixation in the Calvin–Benson cycle[1]. They have evolved to cope with rapid fluctuations in light[2] and inorganic
40 carbon (Ci)[3] availability in their native habitats. When absorbed light exceeds the CO_2 assimilation capacity,
41 the formation of harmful reactive oxygen species can lead to severe cell damage; this is prevented by the
42 activation of photoprotective mechanisms, collectively called non-photochemical quenching (NPQ). NPQ
43 encompasses several processes that are distinguished in terms of their timescales[2], among which the rapidly
44 reversible energy-quenching (qE) is, under most circumstances, the predominant NPQ component[2,4]. The
45 major molecular effector of qE in the green model microalga *Chlamydomonas reinhardtii* (hereafter
46 *Chlamydomonas*) is the LIGHT HARVESTING COMPLEX STRESS RELATED protein LHCSR3, encoded by the
47 *LHCSR3.1* and *LHCSR3.2* genes[5] that slightly differ only in their promoters; LHCSR1 can also contribute
48 significantly to qE under conditions where LHCSR3 is not expressed[6,7]. PSBS, the key qE effector protein in
49 higher plants[8] is encoded in two highly similar paralogues *PSBS1* and *PSBS2* in *Chlamydomonas*[9]. They are
50 only transiently expressed in *Chlamydomonas* under high light (HL)[9,10] and their gene products accumulate
51 under UV-B irradiation[11]; while their precise contribution in *Chlamydomonas* photoprotective responses is
52 still a matter of ongoing research, current understanding is that PSBS proteins contribute to photoprotection
53 during HL acclimation of *Chlamydomonas* through both NPQ-independent and NPQ-dependent mechanisms[12].

54 Intracellular levels of CO_2 are modulated by the availability of its gaseous and hydrated forms[3] in the culture
55 media and the supply of acetate, that is partly metabolized into CO_2[7,13]. Under low CO_2, *Chlamydomonas*
56 activates the CO_2-concentrating mechanism (CCM) to avoid substrate-limitation of photosynthesis by raising
57 the CO_2 concentration at the site of RuBisCO, where CO_2 is assimilated[3]. The CCM mainly comprises of
58 carbonic anhydrases (CAHs) and of inorganic carbon transporters. Almost all CCM-related genes are under
59 the control of the nucleus-localized zinc-finger type nuclear factor CIA5 (aka CCM1)[14-16], including the Myb
60 Transcription Factor LOW-CO_2 -STRESS RESPONSE 1 (LCR1) that controls expression of genes coding for the
61 periplasmic CAH1, the plasma membrane-localized bicarbonate transporter LOW CO_2-INDUCED 1 (LCI1), and
62 the low-CO_2 responsive LCI6, whose role remains to be elucidated[17]. CIA5 is also a major qE regulator
63 activating transcription of genes encoding LHCSR3 and PSBS, while repressing accumulation of LHCSR1
64 protein[7].

65 LHCSR3 expression relies on blue light perception by the photoreceptor phototropin (PHOT)[18], on calcium
66 signaling, mediated by the calcium sensor CAS[19] and on active photosynthetic electron flow[18-20], likely via
67 indirectly impacting CO_2 availability[7]. The critical importance of CO_2 in LHCSR3 expression is demonstrated by

68 the fact that changes in CO_2 concentration can trigger LHCSR3 expression[21-23] even in the absence of light[7].
69 Accumulation of *LHCSR1* and *PSBS* mRNA is under control of the UV-B photoreceptor UVR8[11] and PHOT[24,25]
70 and is photosynthesis-independent[20,25]. While LHCSR1 is CO_2/CIA5 independent at the transcript level[7,25], PSBS
71 is responsive to CO_2 abundance and is under partial control of CIA5[7]. A Cullin (CUL4) dependent E3-ligase[24,26,27]
72 has been demonstrated to post-translationally regulate the transcription factor (TF) complex of CONSTANS
73 (CrCO)[26] and NF-Y isomers[27], which bind to DNA to regulate the transcription of *LHCSR1*, *LHCSR3*, and *PSBS*.
74 The putative TF and diurnal timekeeper RHYTHM OF CHLOROPLAST 75 (ROC75) was shown to repress LHCSR3
75 under illumination with red light[28].

76 Here, we employed a large compendium of RNAseq data from *Chlamydomonas* to build a gene regulatory
77 network (GRN) underlying light and carbon responses, and thus reveal the transcriptional regulation of qE at
78 the interface of these responses. The successful usage of RNAseq data to infer GRNs has been demonstrated
79 in many studies[29-31], although the data pose some challenges that require careful consideration. All of the
80 developed approaches to infer a GRN quantify the interdependence between the transcript levels of TF-
81 coding genes and their putative targets; the resulting prediction model serves as a proxy for the regulatory
82 strength that the product of the TF-coding gene exerts on its target(s). It is usually the case that the number
83 of observations (samples) used in building the model is considerably smaller than the number of TFs used as
84 predictors, leading to collinearity of the transcript levels and associated computational instabilities;
85 furthermore, as an artifact of the computational techniques, some of the inferred regulations may be
86 spurious[32-34]. To address these issues, here we took advantage of combining the outcome of multiple
87 regularization techniques and post-processing to increase the robustness of identified interactions[33-35]. In
88 contrast to our approach, the existing predicted GRNs of *Chlamydomonas* either focused on nitrogen
89 starvation[36] or used a broad RNAseq data compendium, not tailored to inferring regulatory interactions
90 underlying responses to particular cues[37]. Moreover, these GRNs were not obtained by combining the
91 outcomes from multiple inference approaches, shown to increase accuracy of predictions[30], and their quality
92 was not gauged against existing knowledge of gene regulatory interactions.

93 We used an RNAseq data compendium of 158 samples (**Supplementary Table 1**) from *Chlamydomonas*
94 cultures exposed to different light and carbon supply as input to seven benchmarked GRN inference
95 approaches that employ complementary inference strategies[29,30] to identify activating and inhibiting
96 regulatory interactions. We assessed the performance of each approach based on a set of curated TF-target
97 gene interactions with experimental evidence from *Chlamydomonas.* Based on this assessment, we
98 integrated the outcome of the five best performing approaches into a unique resource, a consensus network

of *Chlamydomonas* light- and carbon-dependent transcriptional regulation. We used the consensus network to reveal regulators of qE genes and demonstrated the quality of predictions by experimentally validating two of the six tested candidates. We show here that LCR1 regulates not only CCM, as previously reported[17], but also qE by activating the expression of LHCSR3, and demonstrate that qE-REGULATOR 7 (QER7), belonging to the SQUAMOSA-PROMOTER BINDING PROTEIN-LIKE gene family, is a repressor of qE and CCM-gene expression. Our work consolidates the extensive co-regulation of CCM and photoprotection[7] based on the untargeted assessment of the obtained genome-scale GRN.

Results

Computationally inferred GRN recovered known regulatory interactions underlying qE and CCM in *Chlamydomonas*

We first aimed to employ published and in-house generated RNAseq data sets capturing the transcriptional responses of *Chlamydomonas* to light and acetate availability to infer the underlying GRN. To this end, we obtained data from two publicly available transcriptomics studies of synchronized chemostat wild-type (WT) cultures grown in a 12h/12h light dark scheme and sampled in 30 min to 2h intervals[38,39]. We combined these with our RNAseq data generated from mixotrophically or autotrophically grown batch cultures of the WT and *phot* mutant acclimated to low light (LL) or exposed to HL (**Methods, Supplementary Table 1**). These data sets capture the expected expression patterns of the key genes involved on CCM and qE (**Fig. 1a, Supplementary Fig. 1**) in response to changes in acetate availability and light intensity. Specifically, we found strong up-regulation of these genes in the light[7,25], and a marked inhibition of *LHCSR3.1/2* and CCM genes by acetate as previously described[7,40].

We employed these data together with a list of 407 transcription factors from protein homology studies[41,42] **(Methods, Supplementary Table 2)**, as input to seven GRN inference approaches to robustly predict TF-target interactions, as shown in benchmark studies[30]. The employed methods infer both activating and inhibiting TF-target interactions. Benchmarking of GRNs usually relies on ground truth data obtained from ChIPseq or transcriptomic profiling of TF mutants. Since to date no such comprehensive data set exists for *Chlamydomonas* we manually curated a list of known, experimentally validated regulatory interactions underlying CCM and qE in *Chlamydomonas*[22,26-28], to assess the quality of GRNs inferred by the different approaches. As negative control, we included the reported lack of effect of the SINGLET OXYGEN RESISTANT 1 (SOR1) TF on *PSBS1* transcript levels in diurnal culture[43] as well as a set of four TFs, designated TF1-4, whose knock-out or overexpression did not affect *LHCSR3.1* transcript levels (**Supplementary Note 1**,

129 **Supplementary Fig. 2**, **Fig. 1b**). When we assessed the predicted ranks, as a measure of confidence assigned
130 to the positive and negative ground truth data, we found that two approaches were clear outliers, showing
131 sensitivity of 0%. More specifically, ARACNE[44] and global silencing[45] are unable to recover any positive
132 literature interactions when using a network density threshold of 10% of all possible TF-TF and TF-target
133 interactions (most prominently observable in the case of LCR1 interactions). Possible reasons for this finding
134 are over-trimming or issues with the validity of the underlying assumptions, as seen in other case studies[46].
135 Since the presence of most gene regulatory interactions is dependent on environmental stimuli, it is
136 considerably easier to experimentally validate the presence of TF-target interactions than to show that they
137 do not take place[47]. Thus, in inferring a consensus GRN we considered the five approaches that were able to
138 recover positive interactions, namely: Graphical Gaussian Models (GGM), Context Likelihood of Relatedness
139 (CLR), Elastic Net regression, Gene Network Inference with Ensemble of Trees (GENIE3), and Network
140 Deconvolution (**Methods**).

141 To obtain insights in the performance of these approaches, we next quantified the variability of ranks for the
142 known TF-target gene interactions. We found that the average standard deviation of the ranks of the TF-
143 target gene interactions within an approach is larger than the average standard deviation for the rank of a TF-
144 target gene interaction across the five approaches (**Supplementary Fig. 3**, **Fig. 1b**). This observation suggested
145 that the properties of a given TF-target gene interaction have a stronger influence on its assigned rank than
146 the inference approach used. More specifically, we noted that the regulation of LHCSR genes by the two NF-
147 Y paralogues and the induction of LCR1 by CIA5 are not recovered by any of the used approaches; this is in
148 line with reports showing that CIA5 is constitutively expressed and regulated post-translationally[16] - not
149 reflected in the transcriptomics data. Further, NF-Y factors that rely on complex formation with CrCO to
150 regulate their targets[27], may also act via unresolved post-translational mechanisms. As mentioned in the
151 introduction, some of the employed approaches use regularization techniques, mitigating effects of
152 collinearity and low sample number, this comes at the cost of increasing the number of false negatives,
153 another reason for the high number of unrecovered interactions previously reported in literature. Importantly,
154 the regulatory interactions of the CCM effector genes *LCI1* and *CAH1* by *LCR1* are assigned very high ranks
155 (top 1%) by the approaches considered in the consensus GRN (except for GGM); moreover, only for the
156 interaction of TF1 and LHCSR3.1 we observe false positives, originating from spurious interactions. The
157 interactions of the other four TFs (**Supplementary Note 1, Supplementary Fig. 2**) are correctly discarded by
158 all approaches, indicating the robustness of the employed approaches (**Fig. 1b**). In addition, we observed that
159 CLR and GENIE3 demonstrated the best performance with respect to the set of known interactions. For
160 instance, they identified the regulation of *LHCSR3.1* by CrCO[26,27] and of *PSBS1* by NF-YB[27] (**Fig. 1b**).

161 Generalization of this ranking beyond the known interactions underlying qE and CCM processes is challenging,
162 due to the lack of genome-scale gold standard, and we therefore opted to combine the results of the five
163 approaches, that showed comparable performance, in the consensus GRN **(Methods, Supplementary Table**
164 **3)** to increase robustness of the predictions. Our analyses of the overlap between the consensus and
165 individual GRNs and the enrichment of TF-TF interactions demonstrated the robustness of the inferred
166 interactions **(Supplementary Note 2, Supplementary Fig. 4)**.

167 **Consensus GRN pinpoints LCR1 as a regulator of qE-related genes**

168 Using the consensus GRN, we inferred direct regulators of *LHCSR* and *PSBS* genes and ranked them according
169 to the score resulting from the Borda method (**Methods**)[30,48]. Mutants were available for four of the top ten
170 of TFs with strongest cumulative regulatory effect on qE-related genes (**Fig. 2a, Supplementary Table 4):** Two
171 knock-out mutants of previously uncharacterized genes were ordered from the CliP library[49], which we
172 termed *qE-regulators 4* and *6* (*qer4*, *qer6*; see **Supplementary Fig. 5** for the genotyping of these mutants).
173 Additionally, we obtained an over-expressor line of the N-acetyltransferase LCI8[21] and the knock-out strain of
174 the known CCM regulator LCR1[17]. We tested for a regulatory effect by switching LL-acclimated mutant strains
175 and their respective WT background to HL for 1h and quantified transcript levels of qE-related genes. Since
176 both the paralogs of *PSBS* as well as of *LHCSR3* show correlation greater than 0.96 over all RNAseq samples
177 used in this study and they additionally have very similar expression profiles quantified by RT-qPCR[50], we only
178 probed the transcripts of *LHCSR3.1* and *PSBS1* via qPCR in the validation assays. For *qer4*, *qer6*, and *lci8-oe*
179 we did not observe an effect on the transcript levels of investigated genes after HL exposure (**Supplementary**
180 **Fig. 6**). Thus, qer4 and qer6 are considered false positive predictions of the GRN, despite the fact that *qer4*
181 accumulated 1.5 times more *LHCSR3.1* under LL than the WT. A review of the closest orthologs of LCI8
182 together with the experimental data indicate that it is likely involved in arginine synthesis[51] and wrongly
183 included as histone acetylase in the list of TFs. Interestingly, LCR1, the highest ranking among the tested
184 regulators showed significantly decreased expression of LHCSR3 at both the gene (three times lower, **Fig. 2b**)
185 and protein level (four times lower, **Fig. 2c, d**) compared to the WT; as a result, *lcr1* developed very low NPQ
186 and qE **(Fig. 2e)**. Interestingly, the *lcr1* mutant over-accumulated LHCSR1 and PSBS both at the transcript and
187 at the protein level (**Fig. 2b-d**); Complementation of *lcr1* with the knocked-out gene (strain *lcr1-C*) restored
188 LHCSR3 gene and protein expression as well as the qE phenotype (**Fig. 2b-e**). Because pre-acclimation
189 conditions impact qE gene expression[25] we conducted independent experiments in which cells were
190 acclimated to darkness before exposure to HL and we obtained very similar results. Our data demonstrated
191 that *lcr1* showed significantly lower expression of LHCSR3 and higher expression of LHCSR1/PSBS at both the

192 gene (**Supplementary Fig. 7a**) and protein level (**Supplementary Fig. 7b,c**), and had lower NPQ and qE
193 (**Supplementary Fig. 7d**) than the WT, although the higher expression levels of the *LHCSR1* gene were not
194 rescued by the complementation with the missing *LCR1* gene (**Supplementary Fig. 7a**). Altogether, our data
195 show that LCR1 is a regulator of qE by activating *LHCSR3.1* transcription and repressing LHCSR1 and PSBS
196 accumulation.

197 Furthermore, we revisited the role of LCR1 in regulating CCM genes[17] by analyzing expression of selected CCM
198 genes in WT, *lcr1* and *lcr1-C* cells shifted from LL or darkness to HL, conditions favoring CCM gene expression[7].
199 We first confirmed that under our experimental conditions *lcr1* could not fully induce *LCI1* (**Supplementary**
200 **Fig. 8a, b**) in accordance to the report of the discovery of LCR1[17]. Our analyses further showed a statistically
201 significant impairment of *lcr1* in inducing genes encoding the Ci transporters LOW-CO_2-INDUCIBLE PROTEIN
202 A (LCIA), HIGH-LIGHT ACTIVATED 3 (HLA3) and BESTROPHINE-LIKE PROTEIN 1 (BST1) as well as the carbonic
203 anhydrase CAH4, when shifted from LL or dark to HL (**Supplementary Fig. 8a, b**), indicating that the role of
204 LCR1 in low-CO_2 gene expression extends beyond the regulation of gene expression of *CAH1*, *LCI1* and *LCI6*[17].

205 **PHOT-specific GRN reveals a novel repressor of qE**

206 The light-dependent induction of LHCSR3 is predominantly mediated by the blue light photoreceptor PHOT[18].
207 To analyze the PHOT-dependent transcriptional regulators, we first inferred a GRN based solely on the
208 RNAseq from samples of *phot* and WT acclimated to LL and after 1h exposure to HL (data set PH,
209 **Supplementary Table 1**) using only the GENIE3 approach, reported to show good performance[46,52] and which
210 is among the best performing approaches in our consensus network. Since the PH experiment contains a low
211 number of samples (12 samples, 4 conditions) the inferred GRN will inevitably suffer from the effects of low
212 statistical power and high collinearity. To mitigate these effects, we decided to only include interactions that
213 are also present in the benchmarked consensus network. By determining the intersection of the two networks,
214 we obtained a GRN that resolves regulatory interactions underlying the transcriptomic changes observed in
215 the *phot* mutant, while borrowing the statistical power of the whole RNAseq compendium. We refer to the
216 resulting network as PHOT-specific GRN (**Methods**, **Supplementary Table 5**).

217 When investigating the top 10 regulators of qE genes in this PHOT-specific GRN the interactions where
218 weighted based on the importance score from GENIE3 (**Supplementary Table 6, Fig. 3a**). Among the
219 interactions in this list of PHOT-dependent regulators, we recovered two known regulators of qE, namely,
220 ROC75[28] and CrCO[26,27](**Fig. 3a**). These observations are in line with an existing hypothesis[24] suggesting that a
221 CUL4-dependent E3-ligase targeting CrCO,[26] acts downstream of PHOT. ROC75 has been previously reported
222 to act independently of the PHOT signal based on qPCR studies of the mutant grown synchronously under

223 different light spectra[28]. In our RNAseq data, gathered under continuous white light, we observed a significant
224 difference in expression levels of ROC75 between WT and *phot* (log2 fold-change = 1.03, adj. p-value =
225 $1.80*10^{-7}$).

226 The fact that several regulators showed larger regulatory strength than CrCO in the PHOT-specific GRN
227 indicates the existence of yet unreported regulators of qE effector genes in the PHOT signaling pathway. This
228 is in line with existing results[26], showing that the knock-out of CrCO is insufficient to fully abolish light-
229 dependent activation of LHCSR3. Following this reasoning we obtained *qer1* and *qer7*, the available regulator
230 candidates mutants, from the CLiP library[49] (for genotyping see **Supplementary Fig. 5**). Our results show
231 higher mRNA levels of LHCSR1 in the *qer1* mutant (**Supplementary Fig. 9**); however, this could not be rescued
232 by ectopic expression of the *QER1* gene in the *qer1* mutant background (**Supplementary Fig. 9**). We found
233 significant upregulation of *LHCSR3.1* gene expression in the *qer7* mutant (1.7 times, **Supplementary Fig. 10a**)
234 also reflected in higher NPQ (**Supplementary Fig. 10b)** and qE levels (**Supplementary Fig. 10c**) which we
235 followed up in more detail. To this end, we ectopically expressed the WT *QER7* gene in the *qer7* mutant and
236 generated the complemented strain *qer7-C* that expressed *QER7* to levels similar to those WT
237 (**Supplementary Fig. 5c**). As a result, the *qer7-C* strain showed reduced *LHCSR3* gene expression, NPQ and qE
238 levels as compared with the *qer7* mutant (**Supplementary Fig. 10a-c**). *LHCSR1* and *PSBS* seemed to be
239 unaffected in the qer7 in these LL to HL transition experiments (**Supplementary Fig. 10a**). As with LCR1, we
240 also performed dark to HL experiments to further characterize the photoprotective responses of *qer7*; under
241 these conditions, *qer7* accumulated significantly more *LHCSR1* (1.7 times) and *PSBS1* (2.2 times) while *LHCSR3*
242 remained unaffected (**Supplementary Fig. 10d**). As in the LL to HL experiments (**Supplementary Fig. 10b, c**)
243 *qer7* showed more NPQ and qE (**Supplementary Fig. 10e, f**). Complementation of *qer7* with the missing *QER7*
244 gene restored all phenotypes (*LHCSR1*, *PSBS*, NPQ, qE; **Supplementary Fig. 10d-f**). These data validated the
245 prediction of QER7 as regulator of qE gene expression (**Fig. 3a**) and indicated that QER7 regulates different
246 subsets of qE genes depending on the pre-acclimation conditions; *LHCSR3* when preacclimated under LL,
247 *LHCSR1* and *PSBS* when pre-acclimation occurs in darkness.

248 Motivated by these findings and given the fact that most of the Chlamydomonas transcriptome undergoes
249 diurnal changes[39] we decided to address the role of QER7 in regulating qE genes under light/dark cycles. We
250 synchronized WT, *qer7* and *qer7-C* cells in 12h L/12h D cycle and exposed them to HL right after the end of
251 the dark phase. Our results revealed that under these conditions QER7 functions as a repressor of all qE-
252 related genes; the *qer7* mutant expresses significantly higher LHCSR3, LHCSR1 and PSBS not only at the gene
253 (**Fig. 3b**) but also at the protein (**Fig. 3c, d**) level, and exhibits higher NPQ and qE (**Fig. 3e**), with all phenotypes

254 rescued in the *qer7-C* complemented line. Previous protein homology studies identified QER7 as Squamosa
255 Binding Protein[53] or bZIP TF[54], and here, we provide the first functional annotation of QER7 as a novel qE
256 regulator.

257 **QER7 co-regulates qE-related and CCM genes**

258 Our findings that the regulatory role of CIA5[7] and LCR1 (**Fig. 2 and Supplementary Fig. 7**) extends beyond
259 CCM to also control qE-related gene expression, prompted us to also inspect the expression levels of CCM
260 genes in synchronized *qer7* cells (**Fig. 4a**). Indeed, for five of these transcripts (*HLA3*, *CAH4*, *BST1*, *LCI1*, *LCIA*)
261 we observed a significant upregulation in *qer7* after HL exposure that was reversed by complementation with
262 the *QER7* gene, indicating that QER7 suppresses expression of CCM genes; the suppression role of QER7 on
263 CCM genes was only observable under HL, conditions that favor CCM gene expression[7] and not in the dark
264 (**Fig. 4a**). We subsequently checked if this regulation is also captured in the GRNs. To this end, we used the
265 CCM genes included in **Fig. 4a** as target genes and predicted the top 10 regulators of these genes using the
266 same method as for the qE regulators (**Methods**). Interestingly, we found LCR1 (**Supplementary Fig. 11a, c**)
267 amongst the top regulators of both, CCM and qE genes, in the consensus network and QER7 in the PHOT-
268 specific network (**Supplementary Fig. 11b, d)**.

269 Led by this observation, we investigated the signaling pathway upstream of QER7. To this end, we quantified
270 *QER7* gene expression in synchronized *phot* cultures and observed that *QER7* is overexpressed in the *phot*
271 mutant, suggesting that PHOT suppresses *QER7* expression (**Fig. 4b**). In contrast to *QER7*, *phot* expressed *LCR1*
272 to levels similar to those in WT (**Fig. 4b**), and the same was true for the *qer7* mutant that also expressed *LCR1*
273 to WT levels (**Fig. 4a**). Further validation that LCR1 and QER7 act on different pathways comes from the fact
274 that although LCR1 is controlled by CIA5[55], QER7 is not (**Fig. 4c)**. Thus, while sharing part of their target genes,
275 the two TFs, LCR1 and QER7, mediate different signals. We captured this distinction in our PHOT-specific
276 network, further underlining the power of the inferred networks.

277 Our findings that QER7 represses CCM gene expression (**Fig. 4a**) naturally raised the question whether the
278 *qer7* mutant has altered CCM function, i.e. altered capacity of the cells to accumulate inorganic carbon (Ci).
279 To address this question, we compared WT and *qer7* cells for their affinity for Ci, under conditions where CCM
280 is not fully induced (LL) and after inducing CCM by acclimation to HL, which leads to mRNA accumulation of
281 CCM-related genes (see for example **Fig. 4a** but also our previous study[7]). Under these conditions no
282 difference could be observed between WT and *qer7* (**Supplementary Fig. 12, Supplementary Table 7**). Our
283 data suggest that PHOT, by repressing *QER7* (**Fig. 4b**), is also involved in the regulation of CCM related gene
284 expression. We investigated this further by quantifying CCM gene expression in WT, *phot* mutant and the

285 complemented line *phot-C*, in the samples collected from the experiment presented in Fig. 4b, i.e.
286 synchronized photoautotrophic cultures shifted to HL right after the end of the dark phase. We first analyzed
287 expression of qE genes that was found as expected[18,24,25] to be under control of PHOT (**Supplementary Fig.**
288 **13a**). We then analyzed expression of the five CCM genes found to be repressed by QER7 (**Fig. 4a**); out of
289 those, *CAH4* and *HLA3* were down-regulated in the *phot* mutant exposed to HL after the end of the dark phase
290 in synchronized cultures (**Supplementary Fig. 13b**) and this phenotype was fully rescued in the *phot-C*
291 complemented line, suggesting a potential involvement of PHOT in regulating expression of CCM-related
292 genes. Nevertheless, the affinity of *phot* for Ci was not different than this of WT (**Supplementary Fig. 14,**
293 **Supplementary Table 7**), in line with previous work reporting CCM to be induced to very similar extent under
294 blue or red illumination[56]. Thus, under our experimental conditions, the role of PHOT and QER7 in regulating
295 CCM is restricted to the transcriptional level. Since the PHOT-QER7 pathway acts independently of the LCR1
296 pathway, both regulating the same subset of CCM genes we tested, it may be not so surprising that neither
297 PHOT nor QER7 impact the affinity for Ci; in both *qer7* and *phot* mutants LCR1 levels are unaffected and
298 therefore the control of LCR1 on CCM may mask any potential effect that PHOT or QER7 might have. Since
299 many known CCM regulatory mechanisms act pots-transcriptionally[57], it is conceivable, that the
300 transcriptional regulation of PHOT and QER7 on their own are not sufficient and rely on integration with other
301 simultaneous signals to clear all roadblocks for full CCM induction under HL.

302 **Genome-scale GRN indicates that photoprotection and CCM are co-regulated**

303 The two qE regulators that we validated in this study also regulate CCM genes. Therefore, we next
304 investigated to what extent the observed coregulation pattern applies to the global, known transcriptional
305 regulation of low CO_2 and light stress responsive genes. To this end, we took advantage of the size of the
306 presented genome-scale GRNs and compiled a list of genes putatively involved in photoprotection
307 (**Supplementary Table 8**) or the CCM (**Supplementary Table 9**); we then extracted the 10 TFs exhibiting the
308 strongest regulatory strength on the genes in the compiled lists. We found six (empirical p-value<0.001,
309 **Methods**) and four (empirical p-value < 0.01) of the top 10 regulators to be shared between these two
310 responses in the consensus **(Fig. 5a, b, Supplementary Table 10**) and the PHOT-specific GRN, respectively
311 (**Figure 5c,d, Supplementary Table 11**). The significant, large number of shared regulators is a strong
312 indication that co-regulation of photoprotective and carbon assimilatory processes is a principal feature of
313 Chlamydomonas' transcriptional regulatory program.

314

315

316 ## Discussion

317 The molecular actors and structure of the transcriptional regulatory mechanisms that shape *Chlamydomonas*'
318 response to differential light and carbon availability are largely unknown, although they are paramount to
319 survival of *Chlamydomonas* and offer valuable targets for biological engineering. Here we set out to elucidate
320 the GRN underlying the response to light and carbon availability by combining the results from five
321 complementary inference approaches and data from 158 RNAseq samples of cultures responding to these
322 cues. In the network inference process for this study, we carefully choose approaches and integration
323 procedures developed to address the inherent difficulties of RNAseq data sets (e.g. collinearity and high
324 number of variables compared to samples). Together with the many post-transcriptional layers of regulation
325 in eukaryotic cells, the task of recovering the true GRN, nevertheless, remains a major challenge of the field
326 of systems biology and this study is no exception.

327 We were able to experimentally validate two of the six novel qE regulators which the GRN predicted and for
328 which KO mutants were available: QER7, suppressing LHCSR3, LHCSR1 and PSBS expression (**Fig. 3**,
329 **Supplementary Fig. 10**), and LCR1, activating LHCSR3 and suppressing LHCSR1 and PSBS expression (**Fig. 2**,
330 **Supplementary Fig. 7**). Both TFs also regulate expression of CCM genes, LCR1 as previously reported[17], QER7
331 as demonstrated in this study (**Fig. 4**), suggesting that the processes of qE and CCM are co-regulated.

332 From the physiological point of view, the interconnection of qE and CCM comes as no surprise; exposure to
333 HL boosts CO_2 fixation rates and results in depletion of intracellular Ci, reflected, for instance, in the
334 expression levels of the CO_2-responsive marker RH1[7]; therefore, HL-exposed cells need to activate not only
335 qE, to protect against photooxidative stress, but also CCM to sustain photosynthetic CO_2 fixation. On the other
336 hand, photooxidative damage is exacerbated by CO_2-limitation; when CO_2 fixation decreases,
337 photosynthetically generated electrons accumulate in the electron chain potentially leading to reactive
338 oxygen species generation[58]. Therefore, acclimation to low-CO_2 availability needs to include not only
339 activation of CCM to elevate CO_2 levels at the site of fixation, but also of protection against photooxidative
340 damage. It was recently shown that overexpression of the bZIP transcription factor BLZ8, resulting in
341 enhanced CCM via overexpression of HLA3, CAH7 and CAH8, conferred enhanced oxidative tolerance
342 triggered by alkaline stress [59]. Although the qE capacity of the BZL8 overexpressing lines was not assessed,
343 this work suggests that CCM and protection from oxidative stress are physiologically interconnected.

344 We complemented the findings of the involvement of LCR1 and QER7 in the regulation of qE and CCM related
345 genes with an unbiased analysis of the genome-scale co-regulation of CCM and photoprotective genes. In this
346 way we observed a significant number of regulators targeting both processes in the inferred consensus GRN
347 as well as the PHOT-specific GRN (**Fig. 5**). This finding is in line with several experimental studies: *LHCSR3*
348 mRNA has been reported to accumulate under low CO_2[21,22] while exposure to HL has been reported to trigger
349 CCM protein[60] and mRNA[7] accumulation. The Chloroplast Calcium Sensor protein CAS initially found to be a
350 qE regulator[19] turned out to also regulate CCM [61], and similarly, CIA5, the master regulator of CCM gene
351 expression[14-16] is also controlling qE gene and protein expression[7]. Our results indicate a set of TFs (**Fig 5, Supp.**
352 **Table 10-11**) that likely act downstream of these different signals and integrate them into a common
353 transcriptional response. Their further characterization is a promising avenue for future research.

354 We found QER7 in the list of PHOT-specific regulators and validated its role experimentally: Expression of
355 *QER7* was repressed by PHOT (**Fig. 4b)** and was CIA5-independent (**Fig. 4c),** while expression of *LCR1* is
356 regulated by CIA5[55] and was found to be PHOT-independent (**Fig. 4b).** Thus, we showed that filtering the
357 consensus network by differential expression data of mutants indeed successfully captures this context-
358 specific regulatory interactions. As far as qE is concerned, qE genes are overexpressed in the *qer7* mutant (**Fig.**
359 **3b**), lacking the repressor QER7, and down-regulated in *phot* mutant (**Supplementary Fig. 13a**),
360 overexpressing the QER7 repressor; as for CCM, QER7 represses expression of all five CCM genes we
361 investigated (**Fig. 4a**), with two of them, *CAH4* and *HLA3*, being down-regulated in the *phot* mutant under HL
362 (**Supplementary Fig. 13b**). Further work is needed to obtain a global understanding of the role of phototropin
363 on the transcriptional regulation of Chlamydomonas CCM, including its observed role in controlling some of
364 the CCM genes in the dark (**Supplementary Fig. 13b**); nevertheless, this suggested link forms an interesting
365 parallel with the convergence of phototropin- and CO_2-mediated signals recently shown to control stomata
366 opening, responsible for CO_2/O_2 exchanges, in the model plant Arabidopsis [62].

367 In summary, we presented three valuable sets of PHOT-specific and general regulators: (i) a set of regulators
368 of qE for which we validated available mutants (**Fig. 2a, Fig. 3a, Supp. Tables 4,6**), (ii) a set of regulators of
369 the core CCM genes analysed via qPCR in **Fig. 4**, in which we recovered QER7 and LCR1 as coregulators of
370 expression for qE and CCM genes (**Supplementary Fig. 11**), and (iii) a set of regulators **(Fig. 5, Suppl. Table**
371 **10-11**) of genes putatively involved in photoprotection or CCM (**Supp. Tables 8-9**), which depicted significant
372 coregulation at a global scale.

373 Led by these predictions we experimentally showed that QER7 acts as a repressor of qE and CCM gene
374 expression, LCR1 is a regulator of qE with a more expanded role on regulating CCM as previously thought and

375 finally introduced a photoreceptor-mediated layer of regulation of CCM gene expression. These results
376 clearly demonstrated that the generated GRN represents a powerful resource for future dissection of the
377 transcriptional regulation of responses of *Chlamydomonas* to light and carbon availability. To allow easy
378 access to this resource, we published an R-shiny webtool (https://github.com/arendma/GRN_web) to query
379 the networks for arbitrary regulators and target genes. We expect that the webtool will prompt more
380 concerted, community-wide efforts in resolving the interactions between other pathways that integrate
381 different environmental cues in *Chlamydomonas*.

382 **Methods**

383 **Transcriptome analysis**

384 We assembled a compendium of RNAseq data (**Supplementary Table 1**) that capture regulation of light-
385 dependent processes by combining in-house produced RNAseq measurements with publicly available data
386 from two studies of densely sampled diurnal cultures of Chlamydomonas[38,39]. For the samples in the acetate
387 time-resolved experiment, adapter sequences were specifically trimmed from raw reads using BBduk[63]
388 (ktrim=r k=30 mink=12 minlen=50). Raw reads of the diurnal transcriptome study from Strenkert et al.[39] were
389 obtained from NCBI GEO database (GSE112394). Reads were aligned to the Chlamydomonas reference
390 transcriptome[64] available from JGI Phytozome (Assembly version 5) using RNA STAR aligner. The BAM files
391 obtained from these measurements were analyzed using HTSeq-count[65] (stranded=reverse) to create raw
392 read count files. The raw read counts from Zones et al.[38] were obtained as .tsv from NCBI GEO (GSE71469).
393 The final data set consists of 158 samples from 62 experimental conditions or time points (**Supplementary**
394 **Table 1**). Genes with less than 1 count per million in at least 9 measurements where discarded and the
395 remainder were voom[64] transformed and normalized using library normalization factors based on the TMM[66]
396 approach as implemented in the R Bioconductor package edgeR[67].

397 **Transcription factor set from comparative genomics**

398 To reduce the set of parameters in our network model, we compiled transcription factor (TF) annotations for
399 the Chlamydomonas genome based on proteome homology studies. We obtained the proteomes and protein
400 IDs of predicted Chlamydomonas TFs from Pérez-Rodríguez et al.[41] Since these predictions were built based
401 on the older Chlamydomonas assembly, we first used the conversion table provided by Phytozome to convert
402 JGI4 to Crev5.6 IDs. For the TFs that could not be recovered by this approach we used the Phytozome BLAST
403 tool to align these sequences against the Crev5.6 proteome (BLASTP, E threshold: -1, comparison matrix:
404 BLOSUM62, word length: 11, number of reported alignments: 5). The reported hits were filtered for sequence

405 identity > 97% and gaps ≤ 1 . If sequences mapped multiple times to the same Crev5.6 gene ID, only the hit
406 alignment closest to the N-terminus of the query sequence was kept. The hit was only accepted if the
407 alignment started at least six residues from the N-terminus of the hit sequence. For Crev5.6 loci that had
408 multiple JGI4 TF queries assigned to them the best hit was selected manually. This set was then extended by
409 the TFs found in the study of Jin et al.[42] and the regulators in the manually curated set of CCM and qE
410 regulatory interactions (**Supplementary Tables 8 and 9**). Using this procedure, we compiled a list of 407
411 Chlamydomonas TFs (**Supplementary Table 2**) to be considered as regulators in the inferred networks.

412 **Gene regulatory network inference**

413 The CLR and ARACNE approach were based on all replicate measurements; for all other inference methods
414 the median from each condition was used as input. All input matrices where standardized gene-wise. If not
415 explicitly stated in the respective paragraph the implementations of all GRN inference approaches were
416 applied with their default settings.

417 ***Graphical Gaussian Models***

418 The network inferred from a Graphical Gaussian model of gene regulation was obtained using the
419 implementation of the partial correlation estimate from Schäfer et al.[34] as implemented in the R GeneNet
420 package. All interactions between TFs and another gene/TF with non-zero partial correlations were included
421 as network edges.

422 ***GENIE3***

423 The random forest-based network from GENIE3 was generated using the R Bioconductor implementation
424 provided by the authors[68]. We used only expression levels of TFs as predictors.

425 ***Elastic net regression***

426 A linear regression based network was obtained using the elastic net algorithm[35]. A model was fit for each
427 gene using the expression levels of all TFs as predictors. The two hyperparameters $\lambda 2$ (quadratic penalty) and
428 s (fraction of L1 norm coefficients) were tuned for each gene model using 6-fold cross validation. The 2D
429 parameter space scanned was $\lambda 2$={0,0.001,0.01,0.05,0.1,0.5,1,1.5,2,10,100} and
430 s={0.1,0.2,0.3,0.4,0.5,0.6,0.7,0.8,0.9}. The R2 value for each model was calculated as

$$R^2 = 1 - \frac{\sum(y-\hat{y})}{var(y)}, \quad (1)$$

431 with y denoting the vector of observed expression values and $\hat{y}$ the model predictions. Models with a negative
432 coefficient of determination ($R2$) value were discarded as regularization artifacts. The results of the remaining
433 models were assembled into a network in which interactions were ranked by regression coefficients β
434 normalized by the maximum absolute coefficient:

$$\tilde{\beta} = \frac{1}{\max_i\{|\beta_i|\}}\beta. \quad (2)$$

435

436 ***CLR and ARACNE***

437 The implementation of mutual information (MI)-based network inference approaches from the R package
438 minet[69] was used. Pairwise MI was estimated based on the Spearman correlation as proposed by Olsen et
439 al.[70]. Two networks were constructed based on these MI estimates. Using the CLR approach[71] non-significant
440 interactions were removed based on the z-scores calculated from the marginal distributions of MI values for
441 each gene pair. Alternatively, the ARACNE algorithm[44] was used to prune the network based on the data
442 processing inequality. For both networks only interactions originating from a TF were taken into consideration
443 and edges were ranked according to the assigned MI value.

444 ***Deconvolution and Silencing***

445 For the two networks based on decomposition of the interaction matrix *G* the Pearson correlation matrix
446 obtained from gene expression values was used as input.

447 The deconvolution approach introduced by Feizi and co-workers[72] was implemented as previously described[46].
448 The eigenvalue scaling factor β was initialized as β=0.9 and iteratively reduced in increments of 0.05 until the
449 largest eigenvector of the direct interaction matrix generated by deconvolution was smaller than 1. Edges
450 were ranked according to the deconvoluted interaction matrix.

451 The Silencing approach as described by Barzel et al.[45] was implemented in R. The proposed approximation of
452 the direct interaction matrix *S* in which spurious interactions are silenced relies on the invers of the observed
453 correlation matrix *G*. In our implementation we used the Moore-Penrose pseudoinverse in case *G* was close
454 to singular. In the resulting network edges were ranked according to the approximated silenced interaction
455 matrix.

456 ***Consensus network construction***

457 To improve network quality[30], we built a consensus network integrating the GRN models inferred by the
458 different approaches introduced above. To this end, we used the Borda count election method[48] whereby the
459 rank *r* of an interaction *I* in the consensus network built on the predictions from *k* approaches is given by
460 arithmetic mean of the ranks in the individual networks

$$r_{consens}(I) = \frac{\sum_{i=1}^{k} r_i(I)}{k}. \quad (3)$$

461 Following the reasoning of Feizi et al. [72] in this integration only the top 10% all possible edges in the GRN
462 (625815) were considered from each individual ranking. For an edge that was not assigned a rank by some
463 approaches, the missing ranks were set to 10% of all possible edges plus one.

464 Using this integration method, we assembled a consensus network based on all approaches to compare
465 predictions from all GRN inference approaches (**Supplementary Fig. 4b**). Due to this comparison and their
466 sensitivity of 0% (**Fig. 1b**) the rankings derived from ARACNE and Silencing were only considered in
467 **Supplementary Fig. 4b** and excluded from the final consensus network used for all other analyses. As with
468 the individual networks returned by the different approaches the consensus network **(Supplemental Table 3)**
469 was trimmed to the top 10% of all possible edges according to the integrated ranks. For predictions of
470 regulators the weight of edges in the final network was set as $r_{consens}^{-1}$, denoting the reciprocal of the
471 interaction rank.

472 **PHOT-specific network**

473 To investigate the PHOT-specific regulatory interactions genes that are differentially expressed between phot
474 mutant and wt under low and high light were inferred. To this end, transcript counts of genes with more than
475 1 count per million in at least four replicates from these conditions (**Supplementary Table 1**) were tested for
476 differential expression using the R packages limma[73], DeSeq2[74], and edgeR[67]. Only genes deemed significant
477 by all three tools after Benjamini-Hochberg correction for a false discovery rate of 0.05 were considered
478 differentially expressed with respect to PHOT mutation

479 In the next step, we focused on the normalized and scaled expression levels from these differentially
480 expressed genes and the previously mentioned conditions, to infer a PHOT-specific GRN using GENIE3. To
481 improve robustness of this network, which was obtained from a comparably sparse data set, we only
482 considered the edges in the intersection with the final consensus network. Again, for both networks only the
483 top 10% of possible edges were taken into account. Therefore, the obtained PHOT-network represents a
484 subnetwork of the final consensus in which edges are weighted by the PHOT-specific GENIE3 importance
485 measure **(Supplementary Table 5)**.

486 **Identification of major regulators**

487 We compiled a manually curated list of possible target genes known to be involved in the processes of qE
488 (*LHCSR1, LHCSR3.1/2, PSBS1/2*), photoprotection (**Supplementary Table 8**), and CCM (**Supplementary Table**
489 **9**). Based on the assumption that major regulators act on several genes important for a biological process,
490 the regulatory strength of a candidate regulator (for the given process) was determined by the sum of edge
491 weights w_{ij}between this regulator and the k genes in the respective target gene set

$$C(TF) = \sum_{j=1}^{k} w_{TFj}. \quad (4)$$

492 **Empirical p-value calculation using Monte-Carlo simulation**

493 The one-sided p-value for the overlap between the regulators of CCM and photoprotective genes was
494 approximated by sampling the overlaps of random gene sets. To this end, we compiled two gene sets with
495 the same cardinality as the curated CCM and photoprotective genes. The genes in these sets where
496 randomly sampled without replacement from all targets in the respective networks. The 10 strongest
497 regulators of these two gene sets where then obtained as previously described and the overlap was
498 calculated as our sample statistic. This process was repeated 10,000 times and an empirical p-value was
499 calculated from the number of iterations, r, where the overlap was higher or equal to the observed value,
500 and the total number of iterations, *n* [75]:

$$p = \frac{r+1}{n+1}. \quad (5)$$

501 **Strains and conditions**

502 *C. reinhardtii* strains were grown under 15 µmol photons m^{-2} s^{-1}) in Tris-acetate-phosphate (TAP) media[76] at
503 23 °C in Erlenmeyer flasks shaken at 125 rpm. For all experiments cells were transferred to Sueoka's high salt
504 medium (HSM)[77] at 1 million cells mL^{-1} and exposed to light intensities as described in the text and figure
505 legends. For the investigation of the impact of acetate on the genome-wide transcriptome, HSM was
506 supplemented with 20 mM sodium acetate. *C. reinhardtii* strain CC-125 mt+ was used as WT. The *phot* mutant
507 (depleted from *PHOT1*; gene ID: Cre03.g199000*), was* previously generated[78] and recently characterized
508 together with its complemented line *phot-C*[25]. The *cia5* mutant (defective in *CIA5*, aka CCM1; geneID:
509 Cre02.g096300; Chlamydomonas Resource Centre strain CC-2702), was previously generated[14] and was used
510 along with its complemented *cia5-C* (ref[7]). For synchronized cultures, the cells were grown in HSM for at least
511 5 days under a 12h light/12h dark cycle (light intensity was set at 15 µmol photons m^{-2} s^{-1}; temperature was
512 18 °C in the dark and 23 °C in the light). All CLiP mutant strains used in this study and their parental strain (CC-
513 4533) were obtained from the CLiP library (REF); *qer1* (LMJ.RY0402.072278), *qer4* (LMJ.RY0402.202963), *qer6*

514 (LMJ.RY0402.162350), *qer7* (LMJ.RY0402.118995). The *lcr1* (strain C44), *lcr1-C* (strain C44-B7) and its parental
515 strain Q30P3 as described in[17] were a kind gift from Hideya Fukuzawa. Before performing phenotyping
516 experiments, we first confirmed that *lcr1* shows no expression of *LCR1* and that this is rescued in the *lcr1-C*
517 strain (**Supplementary Fig. 15a**). The *lci8* overexpressing line was purchased from the Chlamydomonas
518 Resource center; strain CSI_FC1G01, expressing pLM005-Cre02.g144800-Venus-3xFLAG in the CC-4533
519 background. Overexpression of LCI8-FLAG was verified by immunoblotting against FLAG (**Supplementary Fig.**
520 **15b**).

521 To complement *qer1*, a 1152 bp genomic DNA fragment from *Chlamydomonas* CC-4533 was amplified by PCR
522 using KOD hot start DNA polymerase (Merck) and primers P11 and P12 (**Supplementary Table 12**). To
523 complement *qer7*, a 5755 bp fragment DNA fragment from *Chlamydomonas* CC-4533 was amplified by PCR
524 with Platinum superfii DNA Polymerase (Thermo Fisher Scientific) and primers P13 and P14 (**Supplementary**
525 **Table 12**). The PCR products were gel purified and cloned into pRAM118[79] by Gibson assembly[80] for
526 expression under control of the *PSAD* promoter. Junctions and insertion were sequenced and constructs were
527 linearized by EcoRV before transformation. Eleven ng/kb of linearized plasmid[81] mixed with 400 µL of 1.0
528 $x10^7$ cells mL^{-1} were electroporated in a volume of 120 mL in a 2-mm-gap electro cuvette using a NEPA21
529 square-pulse electroporator (NEPAGENE, Japan). The electroporation parameters were set as follows: Poring
530 Pulse (300V; 8 ms length; 50 ms interval; one pulse; 40% decay rate; + Polarity), Transfer Pluse (20V; 50 ms
531 length; 50 ms interval; five pulses; 40% decay rate; +/- Polarity). Transformants were selected onto solid agar
532 plates containing 20 µg/ml hygromycin and screened for fluorescence by using a Tecan fluorescence
533 microplate reader (Tecan Group Ltd., Switzerland). Parameters used were as follows: YFP (excitation 515/12
534 nm and emission 550/12 nm) and chlorophyll (excitation 440/9 nm and 680/20 nm). Transformants showing
535 high YFP/chlorophyll value were further analyzed by real time qPCR.

536 Unless otherwise stated, LL conditions corresponded to 15 µmol photons m^{-2} s^{-1} while HL conditions
537 corresponded to 300 µmol photons m^{-2} s^{-1} of white light (Neptune L.E.D., France; see[7] for light spectrum). All
538 experiments were repeated at least three times to verify their reproducibility.

539 **DNA Isolation and genotyping of CLiP mutants.**

540 Total genomic DNA from CLiP mutants and corresponding wild-type strain CC-4533 was extracted according
541 to the protocol suggested by CLiP website (https://www.chlamylibrary.org/). One µl of the extracted DNA was
542 used as a template for the PCR assays, using Phire Plant Direct PCR polymerase (Thermo Fisher Scientific). To
543 confirm the CIB1 insertion site in the CLiP mutants, gene-specific primers were used that anneal upstream
544 and downstream of the predicted insertion site of the cassette (primer pairs P3-P4, P7-P8, P9-P10 and P5-P6

545 for *qer6*, *qer1*, *qer7* and *qer4* respectively*;* **Supplementary Table 12**). While all these primers worked in DNA
546 extracted from WT, they did not work in the DNA extracted from the mutants, with the exception of *qer4*
547 (**Supplementary Fig. 5**), therefore primers specific for the 5' and 3' ends of the CIB1 Cassette were additionally
548 used. All the primers used for genotyping were shown in **Supplementary Table 12**. We further confirmed the
549 disruption of the genes of interest by quantifying their mRNA accumulation (**Supplementary Fig. 5**).

550 **mRNA quantification**

551 Total RNA was extracted using the RNeasy Mini Kit (Qiagen) and treated with the RNase-Free DNase Set
552 (Qiagen). 1 µg total RNA was reverse transcribed with oligo dT using Sensifast cDNA Synthesis kit (Meridian
553 Bioscience, USA). qPCR reactions were performed and quantified in a Bio-Rad CFX96 system using
554 SsoAdvanced Universal SYBR Green Supermix (BioRad). The primers (0.3 µM) used for qPCR are listed in
555 **Supplementary Table 13**. A gene encoding G protein subunit-like protein (GBLP)[82] was used as the
556 endogenous control , and relative expression values relative to *GBLP* were calculated from three biological
557 replicates, each of which contained three technical replicates. All primers using for qPCR (**Supplementary**
558 **Table 13**) were confirmed as having at least 90% amplification efficiency. In order to conform mRNA
559 accumulation data to the distributional assumptions of ANOVA, i.e. the residuals should be normally
560 distributed and variances should be equal among groups, Two-Way Analysis of Variance were computed with
561 log-transformed data $Y = \log X$ where X is mRNA accumulation[83].

562 **Immunoblotting**

563 Protein samples of whole cell extracts (0.5 µg chlorophyll or 10 µg protein) were loaded on 4-20% SDS-PAGE
564 gels (Mini-PROTEAN TGX Precast Protein Gels, Bio-Rad) and blotted onto nitrocellulose membranes. Antisera
565 against LHCSR1 (AS14 2819), LHCSR3 (AS14 2766), ATPB (AS05 085), CAH4/5 (AS11 1737) were from Agrisera
566 (Vännäs, Sweden); antiserum against PSBS was from ShineGene Molecular Biotech (Shanghai, China)
567 targeting the peptides described in Ref.[9]. ATPB was used as a loading control. An anti-rabbit horseradish
568 peroxidase–conjugated antiserum was used for detection. The blots were developed with ECL detection
569 reagent, and images of the blots were obtained using a CCD imager (ChemiDoc MP System, Bio-Rad). For the
570 densitometric quantification, data were normalized with ATPB.

571 **Fluorescence-based measurements**

572 Fluorescence-based photosynthetic parameters were measured with a a pulse modulated amplitude
573 fluorimeter (MAXI-IMAGING-PAM, HeinzWaltz GmbH, Germany). Prior to the onset of the measurements,
574 cells were acclimated to darkness for 15 min. Chlorophyll fluorescence was recorded during 10 min under 570

575 µmol m^{-2} s^{-1} of actinic blue light followed by finishing with 10 min of measurements of fluorescence relaxation
576 in the dark. A saturating pulse (200 msec) of blue light (6000 µmol photons m^{-2} sec^{-1}) was applied for
577 determination of Fm (the maximal fluorescence yield in dark-adapted state) or Fm' (maximal fluorescence in
578 any light-adapted state). NPQ was calculated as (*F*m – *F*m')/*F*m' based on[84]; qE was estimated as the fraction
579 of NPQ that is rapidly inducible in the light and reversible in the dark.

580 **CO_2-dependent O_2 evolution**

581 The measurements were performed in accordance with [85] with minor modifications. Cells in photoautotrophic
582 conditions (Sueoka's high salt medium; HSM[77]), shaken in Erlenmeyer flasks at 125 rpm and 23 °C were shifted
583 from LL (overnight at 15 µmol m^{-2} s^{-1}) to HL (4h at 300 µmol m^{-2} s^{-1}) in order to induce the CCM. Cells were
584 suspended in 4ml 25 mM HEPES-KOH buffer (pH 7.3), at 25 µg chlorophyll per mL and were briefly sparged
585 with nitrogen gas to remove the dissolved inorganic carbon (Ci). The cells were then transferred to an oxygen
586 respiration vial (Pyro Science GmbH, Aachen, Germany) and were illuminated at 300 µmol photons m^{-2} s^{-1} for
587 about 10-20 minutes, until no net oxygen evolution was seen, an indication that the internal Ci was depleted.
588 Ci concentration in the cell suspension was then increased by stepwise injecting $NaHCO_3$ with a microsyringe.
589 O_2 evolution was measured using a fiber optic probe (FireStingO2, Pyro Science GmbH, Aachen, Germany).
590 Cumulative concentration of $NaHCO_3$ after each addition were as follows: 25, 50, 100, 250, 500, 1000, 2000
591 µM. $K_{1/2}$(Ci), the Ci concentration needed for half maximal rate of oxygen evolution, and Vmax were calculated
592 by non-linear curve fitting to the Michaelis-Menten equation, using Prism Graph (GraphPad Software, LLC).

593 **Data and material availability**

594 The consensus and PHOT-specific GRN are contained in edge list format as Supplemental Table 3 and
595 Supplemental Table 5, respectively. To allow easy access to the information, we developed an R-shiny webtool
596 that allows to query arbitrary TFs and target genes for regulatory interactions. The R-shiny webtool can be
597 accessed at https://github.com/arendma/GRN_web. The code for GRN inference is available at
598 https://github.com/arendma/GRN_code. The source data underlying Figures 2-4 and Supplementary Figures
599 2, 5c, 6, 7, 8, 9, 10, 12, 13, 14 and 15 are provided as a Source Data file. All biological material described in
600 this study is available upon request.

601 **References**

602 1. Eberhard, S., Finazzi, G. & Wollman, F. A. The dynamics of photosynthesis. *Annu. Rev. Genet.* **42,**
603 463–515 (2008).
604 2. Erickson, E., Wakao, S. & Niyogi, K. K. Light stress and photoprotection in Chlamydomonas
605 reinhardtii. *Plant J.* **82,** 449–465 (2015).
606 3. Moroney, J. V. & Ynalvez, R. A. Proposed carbon dioxide concentrating mechanism in
607 Chlamydomonas reinhardtii. *Eukaryotic Cell* **6,** 1251–1259 (2007).
608 4. Niyogi, K. K. PHOTOPROTECTION REVISITED: Genetic and Molecular Approaches. *Annu. Rev. Plant*
609 *Physiol. Plant Mol. Biol.* **50,** 333–359 (1999).
610 5. Peers, G. *et al.* An ancient light-harvesting protein is critical for the regulation of algal
611 photosynthesis. *Nature* **462,** 518–521 (2009).
612 6. Dinc, E. *et al.* LHCSR1 induces a fast and reversible pH-dependent fluorescence quenching in LHCII in
613 Chlamydomonas reinhardtii cells. *Proc. Natl. Acad. Sci. U.S.A.* **113,** 7673–7678 (2016).
614 7. Ruiz-Sola, M. *et al.* Photoprotection is regulated by light-independent CO2 availability. *bioRxiv*
615 (2021). Doi:10.1101/2021.10.23.465040
616 8. Li, X. P. *et al.* A pigment-binding protein essential for regulation of photosynthetic light harvesting.
617 *Nature* **403,** 391–395 (2000).
618 9. Correa-Galvis, V. *et al.* Photosystem II Subunit PsbS Is Involved in the Induction of LHCSR Protein-
619 dependent Energy Dissipation in Chlamydomonas reinhardtii. *J. Biol. Chem.* **291,** 17478–17487
620 (2016).
621 10. Tibiletti, T., Auroy, P., Peltier, G. & Caffarri, S. Chlamydomonas reinhardtii PsbS Protein Is Functional
622 and Accumulates Rapidly and Transiently under High Light. *Plant Physiol.* **171,** 2717–2730 (2016).
623 11. Allorent, G. *et al.* UV-B photoreceptor-mediated protection of the photosynthetic machinery in
624 Chlamydomonas reinhardtii. *Proc. Natl. Acad. Sci. U.S.A.* **113,** 14864–14869 (2016).
625 12. Redekop, P. *et al.* PsbS contributes to photoprotection in Chlamydomonas reinhardtii independently
626 of energy dissipation. *Biochimica et Biophysica Acta (BBA) – Bioenergetics* **1861,** 148183 (2020).
627 13. Hanawa, Y., Watanabe, M., Karatsu, Y., Fukuzawa, H. & Shiraiwa, Y. Induction of a high-CO2-
628 inducible, periplasmic protein, H43, and its application as a high-CO2-responsive marker for study of
629 the high-CO2-sensing mechanism in Chlamydomonas reinhardtii. *Plant Cell Physiol.* **48,** 299–309
630 (2007).
631 14. Moroney, J. V. *et al.* Isolation and Characterization of a Mutant of Chlamydomonas reinhardtii
632 Deficient in the CO2 Concentrating Mechanism. *Plant Physiol.* **89,** 897–903 (1989).
633 15. Fukuzawa, H. *et al.* Ccm1, a regulatory gene controlling the induction of a carbon-concentrating
634 mechanism in Chlamydomonas reinhardtii by sensing CO2 availability. *Proc. Natl. Acad. Sci. U.S.A.* **98,**
635 5347–5352 (2001).
636 16. Xiang, Y., Zhang, J. & Weeks, D. P. The Cia5 gene controls formation of the carbon concentrating
637 mechanism in Chlamydomonas reinhardtii. *Proc. Natl. Acad. Sci. U.S.A.* **98,** 5341–5346 (2001).
638 17. Yoshioka, S. *et al.* The novel Myb transcription factor LCR1 regulates the CO2-responsive gene Cah1,
639 encoding a periplasmic carbonic anhydrase in Chlamydomonas reinhardtii. *Plant Cell* **16,** 1466–1477
640 (2004).
641 18. Petroutsos, D. *et al.* A blue-light photoreceptor mediates the feedback regulation of photosynthesis.
642 *Nature* **537,** 563–566 (2016).
643 19. Petroutsos, D. *et al.* The chloroplast calcium sensor CAS is required for photoacclimation in
644 *Chlamydomonas reinhardtii*. *Plant Cell* **23,** 2950–2963 (2011).
645 20. Maruyama, S., Tokutsu, R. & Minagawa, J. Transcriptional regulation of the stress-responsive light
646 harvesting complex genes in *Chlamydomonas reinhardtii*. *Plant Cell Physiol.* **55,** 1304–1310 (2014).

21. Miura, K. *et al.* Expression profiling-based identification of CO2-responsive genes regulated by CCM1 controlling a carbon-concentrating mechanism in Chlamydomonas reinhardtii. *Plant Physiol.* **135,** 1595–1607 (2004).
22. Fang, W. *et al.* Transcriptome-wide changes in Chlamydomonas reinhardtii gene expression regulated by carbon dioxide and the CO2-concentrating mechanism regulator CIA5/CCM1. *Plant Cell* **24,** 1876–1893 (2012).
23. Brueggeman, A. J. *et al.* Activation of the carbon concentrating mechanism by CO2 deprivation coincides with massive transcriptional restructuring in Chlamydomonas reinhardtii. *Plant Cell* **24,** 1860–1875 (2012).
24. Aihara, Y., Fujimura-Kamada, K., Yamasaki, T. & Minagawa, J. Algal photoprotection is regulated by the E3 ligase CUL4-DDB1DET1. *Nature Plants* **5,** 34–40 (2019).
25. Redekop, P. *et al.* Transcriptional regulation of photoprotection in dark-to-light transition- more than just a matter of excess light energy. *Sci Adv* (2022).
26. Gabilly, S. T. *et al.* Regulation of photoprotection gene expression in Chlamydomonas by a putative E3 ubiquitin ligase complex and a homolog of CONSTANS. *Proc. Natl. Acad. Sci. U.S.A.* **116,** 17556–17562 (2019).
27. Tokutsu, R., Fujimura-Kamada, K., Matsuo, T., Yamasaki, T. & Minagawa, J. The CONSTANS flowering complex controls the protective response of photosynthesis in the green alga Chlamydomonas. *Nat Comms* **10,** 655–10 (2019).
28. Kamrani, Y. Y., Matsuo, T., Mittag, M. & Minagawa, J. ROC75 is an Attenuator for the Circadian Clock that Controls LHCSR3 Expression. *Plant Cell Physiol.* **59,** 2602–2607 (2018).
29. Omranian, N., Eloundou-Mbebi, J. M. O., Mueller-Roeber, B. & Nikoloski, Z. Gene regulatory network inference using fused LASSO on multiple data sets. *Sci Rep* **6,** 1–14 (2016).
30. Marbach, D. *et al.* Wisdom of crowds for robust gene network inference. *Nat. Methods* **9,** 796–804 (2012).
31. Fang, L. *et al.* GRNdb: Decoding the gene regulatory networks in diverse human and mouse conditions. *Nucl. Acids Res.* **49,** D97–D103 (2021).
32. Omranian, N. & Nikoloski, Z. in *Methods in Molecular Biology* **1629,** 283–295 (2017).
33. Huynh-Thu, V. A. & Sanguinetti, G. in *Methods in Molecular Biology* **1883,** 1–23 (2019).
34. Schäfer, J. & Strimmer, K. A shrinkage approach to large-scale covariance matrix estimation and implications for functional genomics. *Stat Appl Genet Mol Biol* **4,** Article32 (2005).
35. Zou, H. & Hastie, T. Regularization and variable selection via the elastic net. *Journal of the Royal Statistical Society: Series B (Statistical Methodology)* **67,** 301–320 (2005).
36. Gargouri, M. *et al.* Identification of regulatory network hubs that control lipid metabolism in Chlamydomonas reinhardtii. *J. Exp. Bot.* **66,** 4551–4566 (2015).
37. Lämmermann, N. *et al.* Ubiquitin ligase component LRS1 and transcription factor CrHy5 act as a light switch for photoprotection in <em>Chlamydomonas</em&gt. *bioRxiv* 2020.02.10.942334 (2020).
38. Zones, J. M., Blaby, I. K., Merchant, S. S. & Umen, J. G. High-Resolution Profiling of a Synchronized Diurnal Transcriptome from Chlamydomonas reinhardtii Reveals Continuous Cell and Metabolic Differentiation. *Plant Cell* **27,** 2743–2769 (2015).
39. Strenkert, D. *et al.* Multiomics resolution of molecular events during a day in the life of Chlamydomonas. *Proc. Natl. Acad. Sci. U.S.A.* **116,** 2374–2383 (2019).
40. Fett, J. P. & Coleman, J. R. Regulation of Periplasmic Carbonic Anhydrase Expression in Chlamydomonas reinhardtii by Acetate and pH. *Plant Physiol.* **106,** 103–108 (1994).
41. Pérez-Rodríguez, P. *et al.* PlnTFDB: Updated content and new features of the plant transcription factor database. *Nucl. Acids Res.* **38,** (2009).

42. Jin, J. *et al.* PlantTFDB 4.0: Toward a central hub for transcription factors and regulatory interactions in plants. *Nucl. Acids Res.* **45,** D1040–D1045 (2017).
43. Fischer, B. B. *et al.* SINGLET OXYGEN RESISTANT 1 links reactive electrophile signaling to singlet oxygen acclimation in Chlamydomonas reinhardtii. *Proc. Natl. Acad. Sci. U.S.A.* **109,** E1302–11 (2012).
44. Margolin, A. A. *et al.* ARACNE: An algorithm for the reconstruction of gene regulatory networks in a mammalian cellular context. *BMC Bioinformatics* **7,** 1–15 (2006).
45. Barzel, B. & Barabási, A.-L. Network link prediction by global silencing of indirect correlations. *Nature Biotechnology* **31,** 720–725 (2013).
46. Omranian, N., Eloundou-Mbebi, J. M. O., Mueller-Roeber, B. & Nikoloski, Z. Gene regulatory network inference using fused LASSO on multiple data sets. *Sci Rep* **6,** 20533 (2016).
47. Cerulo, L., Elkan, C. & Ceccarelli, M. Learning gene regulatory networks from only positive and unlabeled data. *BMC Bioinformatics* **11,** 228–16 (2010).
48. de Borda, J.-C. Mémoire sur les élections au scrutin. *Histoire de l'Academie Royale des Sciences* (1781).
49. Li, X. *et al.* A genome-wide algal mutant library and functional screen identifies genes required for eukaryotic photosynthesis. *Nat. Genet.* **51,** 627–635 (2019).
50. Redekop, P. *et al.* Transcriptional regulation of photoprotection in dark-to-light transition-More than just a matter of excess light energy. *Sci Adv* **8,** (2022).
51. UniProt Consortium. UniProt: the universal protein knowledgebase in 2021. *Nucleic Acids Res.* **49,** D480–D489 (2021).
52. Marbach, D. *et al.* Wisdom of crowds for robust gene network inference. *Nat. Methods* **9,** 796–804 (2012).
53. Mi, H. *et al.* PANTHER version 16: A revised family classification, tree-based classification tool, enhancer regions and extensive API. *Nucl. Acids Res.* **49,** D394–D403 (2021).
54. Thiriet-Rupert, S. *et al.* Transcription factors in microalgae: genome-wide prediction and comparative analysis. *BMC Genomics* **17,** 282 (2016).
55. Yoshioka, S. *et al.* The novel Myb transcription factor LCR1 regulates the CO2-responsive gene Cah1, encoding a periplasmic carbonic anhydrase in Chlamydomonas reinhardtii. *Plant Cell* **16,** 1466–1477 (2004).
56. Borodin, V. B. Effect of red and blue light on acclimation of Chlamydomonas reinhardtii to CO2-limiting conditions. *Russian Journal of Plant Physiolofy* **55,** 441–448 (2008).
57. Santhanagopalan, I., Wong, R., Mathur, T. & Griffiths, H. Orchestral manoeuvres in the light: crosstalk needed for regulation of the Chlamydomonas carbon concentration mechanism. *J. Exp. Bot.* **72,** 4604–4624 (2021).
58. Chaux, F., Peltier, G. & Johnson, X. A security network in PSI photoprotection: regulation of photosynthetic control, NPQ and O2 photoreduction by cyclic electron flow. *Front Plant Sci* **6,** 875 (2015).
59. Choi, B. Y. *et al.* The Chlamydomonas bZIP transcription factor BLZ8 confers oxidative stress tolerance by inducing the carbon-concentrating mechanism. *Plant Cell* **34,** 910–926 (2022).
60. Scholz, M. *et al.* Light-dependent N-terminal phosphorylation of LHCSR3 and LHCB4 are interlinked in Chlamydomonas reinhardtii. *Plant J.* **99,** 877–894 (2019).
61. Wang, L. *et al.* Chloroplast-mediated regulation of CO2-concentrating mechanism by Ca2+-binding protein CAS in the green alga Chlamydomonas reinhardtii. *Proc. Natl. Acad. Sci. U.S.A.* **113,** 12586–12591 (2016).
62. Hiyama, A. *et al.* Blue light and CO2 signals converge to regulate light-induced stomatal opening. *Nat Comms* **8,** 1284 (2017).

741 63. Bushnell, B. BBMap: A Fast, Accurate, Splice-Aware Aligner. *Lawrence Berkeley National Laboratory.*
742 *LBNL Report LBNL-E* (2014).
743 64. Law, C. W., Chen, Y., Shi, W. & Smyth, G. K. Voom: Precision weights unlock linear model analysis
744 tools for RNA-seq read counts. *Genome Biology* **15,** 1–17 (2014).
745 65. Anders, S., Pyl, P. T. & Huber, W. HTSeq-A Python framework to work with high-throughput
746 sequencing data. *Bioinformatics* **31,** 166–169 (2015).
747 66. Robinson, M. D. & Oshlack, A. A scaling normalization method for differential expression analysis of
748 RNA-seq data. *Genome Biology* **11,** 1–9 (2010).
749 67. Robinson, M. D., McCarthy, D. J. & Smyth, G. K. edgeR: A Bioconductor package for differential
750 expression analysis of digital gene expression data. *Bioinformatics* **26,** 139–140 (2009).
751 68. Huynh-Thu, V. A., Irrthum, A., Wehenkel, L. & Geurts, P. Inferring regulatory networks from
752 expression data using tree-based methods. *PloS ONE* **5,** e12776 (2010).
753 69. Meyer, P. E., Lafitte, F. & Bontempi, G. Minet: A r/25einhardtii25 package for inferring large
754 transcriptional networks using mutual information. *BMC Bioinformatics* **9,** 1–10 (2008).
755 70. Olsen, C., Meyer, P. E. & Bontempi, G. On the impact of entropy estimation on transcriptional
756 regulatory network inference based on mutual information. *Eurasip Journal on Bioinformatics and*
757 *Systems Biology* **2009,** (2009).
758 71. Faith, J. J. *et al.* Large-scale mapping and validation of Escherichia coli transcriptional regulation from
759 a compendium of expression profiles. *PloS Biol.* **5,** 0054–0066 (2007).
760 72. Feizi, S., Marbach, D., Médard, M. & Kellis, M. Network deconvolution as a general method to
761 distinguish direct dependencies in networks. *Nature Biotechnology* **31,** 726–733 (2013).
762 73. Ritchie, M. E. *et al.* Limma powers differential expression analyses for RNA-sequencing and
763 microarray studies. *Nucl. Acids Res.* **43,** e47 (2015).
764 74. Love, M. I., Huber, W. & Anders, S. Moderated estimation of fold change and dispersion for RNA-seq
765 data with DESeq2. *Genome Biology* **15,** 1–21 (2014).
766 75. North, B. V., Curtis, D. & Sham, P. C. A note on the calculation of empirical P values from Monte Carlo
767 procedures [1]. *American Journal of Human Genetics* **71,** 439–441 (2002).
768 76. Gorman, D. S. & Levine, R. P. Cytochrome f and plastocyanin: their sequence in the photosynthetic
769 electron transport chain of *Chlamydomonas 25einhardtii*. *Proc. Natl. Acad. Sci. U.S.A.* **54,** 1665–1669
770 (1965).
771 77. Sueoka, N. Mitotic replication of deoxyribonucleic acid in *Chlamydomonas 25einhardtii*. *Proc. Natl.*
772 *Acad. Sci. U.S.A.* **46,** 83–91 (1960).
773 78. Greiner, A. *et al.* Targeting of Photoreceptor Genes in Chlamydomonas reinhardtii via Zinc-Finger
774 Nucleases and CRISPR/Cas9. *Plant Cell* **29,** 2498–2518 (2017).
775 79. Kaye, Y. *et al.* The mitochondrial alternative oxidase from Chlamydomonas reinhardtii enables
776 survival in high light. *J. Biol. Chem.* **294,** 1380–1395 (2019).
777 80. Gibson, D. G. *et al.* Enzymatic assembly of DNA molecules up to several hundred kilobases. *Nat.*
778 *Methods* **6,** 343–345 (2009).
779 81. Mackinder, L. C. M. *et al.* A repeat protein links Rubisco to form the eukaryotic carbon-concentrating
780 organelle. *Proc. Natl. Acad. Sci. U.S.A.* **113,** 5958–5963 (2016).
781 82. Schloss, J. A. A Chlamydomonas gene encodes a G protein beta subunit-like polypeptide. *Molec. Gen.*
782 *Genet.* **221,** 443–452 (1990).
783 83. Schlesselman, J. J. Data Transformation in Two-Way Analysis of Variance. *Journal of the American*
784 *Statistical Association* (2012). Doi:10.1080/01621459.1973.10482435
785 84. Genty, B., Briantais, J.-M. & Baker, N. R. The relationship between the quantum yield of
786 photosynthetic electron transport and quenching of chlorophyll fluorescence. *Biochimica et*
787 *Biophysica Acta (BBA)* **990,** 87–92 (1989).

788 85. Mukherjee, A. *et al.* Thylakoid localized bestrophin-like proteins are essential for the CO2
789 concentrating mechanism of Chlamydomonas reinhardtii. *Proc. Natl. Acad. Sci. U.S.A.* **116,** 16915–16920
790 (2019).

791

Acknowledgments

We are grateful to Prof. Hideya Fukuzawa for sending us *lcr1*, *lcr1-C* and their respective WT strains and to Prof. Peter Jahns for the antibody against PSBS.

Funding:

The authors would like to thank the following agencies for funding: The Human Frontiers Science Program through the funding of the project RGP0046/2018 (DP, ZN); the French National Research Agency in the framework of the Young Investigators program ANR-18-CE20-0006 through the funding of the project MetaboLight (DP); the French National Research Agency in the framework of the Investissements d'Avenir program ANR-15-IDEX-02, through the funding of the "Origin of Life" project of the Univ. Grenoble-Alpes (DP, YY); the French National Research Agency through the funding of the Grenoble Alliance for Integrated Structural & Cell Biology GRAL project ANR-17-EURE-0003 (DP, MAR-S), the Prestige Marie-Curie co-financing grant PRESTIGE-2017-1-0028 (MAR-S); the International Max Planck Research School 'Primary Metabolism and Plant Growth' at the Max Planck Institute of Molecular Plant Physiology (MA, ZN).

Competing interests: Authors declare that they have no competing interests.

Figures

Fig. 1: Characterization of the consensus GRN inferred by employing a compendium of RNA-seq data from diverse light and culture conditions. **A.** Expression levels of representative CCM and qE genes are plotted over all samples used for network inference (z-scaled log values are depicted). The column annotation gives information on the culture conditions and data set (see also **Supplementary Table 1**); no clustering was applied. **Supplementary Fig. 1** shows an enlarged version of this figure with sample names included. **B.** The heatmap rows correspond to experimentally validated or invalidated (neg) gene regulatory interactions involved in qE and CCM, curated from literature. The heatmap indicates ranking of these interactions by different approaches and the consensus network. Edges are considered highly ranked (depicted in blue) if they are above the 10% network density threshold. Edges ranked below this threshold are depicted in red. Edges that were not included in the given network are marked in grey. At the bottom of the heatmap the relative number of edges inferred by each approach is provided. ARACNE and Silencing columns were only plotted for comparison and were not used in building the consensus GRN (see Methods). TF1: MYB-like DNA-binding protein, Cre01.g034350; TF2: RWP8, RWP-RK transcription factor, Cre04.g218050; TF3: RWP5, RWP-RK transcription factor, Cre06.g285600; TF4: bHLH domain-containing protein, Cre07.g349152)

Fig. 2: Consensus GRN for light and acetate responses pinpoints LCR1 as regulator of qE-related genes. A. Dot plot of the relative regulatory strength of the top 10 regulators of qE-related genes in the consensus GRN (see Methods). TFs are marked in green if qE transcript levels were affected in the respective knock-out strain and this effect was reversed by complementation with the missing gene. TFs for which no effect was observed are marked in red. TFs for which no mutant lines were available are plotted in grey. **B.** WT, *lcr1* and *lcr1-C* cells were acclimated for 16h in LL (15 µmol photons m^{-2} s^{-1}). After sampling for the LL conditions, light intensity was increased to 300 µmol photons m^{-2} s^{-1} (HL); samples were taken 1 h (RNA) or 4 h (protein and photosynthetic measurements) after exposure to HL. Shown are relative expression levels of qE-related genes at the indicated conditions normalized to WT LL (*n* = 3 biological samples, mean ± sd). **C**. Immunoblot analyses of LHCSR1, LHCSR3, PSBS and ATPB (loading control) of one of the three biological replicates, under the indicated conditions. **D.** Quantification of immunoblot data of all replicates in panel **c** after normalization to ATPB. Shown are the HL treated samples; WT protein levels were set as 1. **E.** NPQ and calculated qE (as an inset) 4h after exposure to HL (*n* = 3 biological samples, mean ± s.d). The p-values for the comparisons are based on ANOVA Dunnett's multiple comparisons test and as indicated in the graphs (*, $P < 0.005$, **, $P < 0.01$, ***, $P < 0.001$, ****, $P < 0.0001$). Statistical analyses for panels **b** and **d** were applied on log10-transformed values.

Fig. 3: Fig. 3: A PHOT-specific GRN pinpoints QER7 as a suppressor of the expression of qE-related genes. A. Dot plot of the relative regulatory strength of the top 10 regulators of qE-related genes in the PHOT-specific GRN (see **Methods**). TFs are marked in green if qE transcript levels were affected in the respective knock-out strain and this effect was reversed by complementation with the knocked-out gene, in yellow, if the effect was not reversed by complementation, and in red, if no mutant effect was observed in the mutant. TFs for which no mutant lines were available are plotted in grey. **B**. WT, *qer7* and *qer7-C* cells were synchronized under 12h light (15 µmol m^{-2} s^{-1})/12h dark cycles. After sampling for the dark conditions (end of the dark phase), cells were exposed to 300 µmol photons m^{-2} s^{-1} (HL); samples were taken 1 h (RNA) or 4 h (protein and photosynthetic measurements) after exposure to HL. Shown are relative expression levels of qE-related genes at the indicated conditions normalized to WT LL (*n* = 3 biological samples, mean ± sd). **C**. Immunoblot analyses of LHCSR1, LHCSR3 and ATPB (loading control) of one of the three biological replicate set of samples, under the indicated conditions. **D.** Quantification of immunoblot data of all replicates in panel **c** after

854 normalization to ATPB. WT protein levels at HL were set as 1. **E.** NPQ and qE, measured 4h after exposure to
855 HL (*n* = 3 biological samples, mean ± sd). The p-values for the comparisons are based on ANOVA Dunnett's
856 multiple comparisons test and are indicated in the graphs (*, P < 0.005, **, P < 0.01, ***, P < 0.001, ****, P <
857 0.0001). Statistical analyses for panel **b** and **d** were applied on log10- transformed values.

858 **Fig. 4: QER7 suppresses transcription of CCM genes and depends on PHOT.** *Qer7*, *phot* and *cia5* cells
859 alongside with their complemented lines (*qer7-C*, *phot-C* and *cia5-C* respectively*) and* WT backgrounds, were
860 synchronized under 12h light (15 µmol m^{-2} s^{-1})/12h dark cycles, in photoautotrophic conditions (Sueoka's high
861 salt medium; HSM), at 23 °C in Erlenmeyer flasks shaken at 125 rpm. After sampling at the end of the dark
862 phase, cells were exposed to 300 µmol photons m^{-2} s^{-1} (HL) and samples were taken 1 h after HL exposure. **A.**
863 Relative expression levels of CCM genes at the indicated conditions. **B** Relative expression levels of *QER7* and
864 *LCR1* in WT, *phot* and *phot-C*. **c** Relative expression levels of *QER7* in WT, *cia5* and *cia5-C.* In all cases (**a**, **b** and
865 **c**) expression levels were normalized to WT LL (*n* = 3 biological samples, mean ± sd). The p-values for the
866 comparisons are based on ANOVA employing Dunnett's multiple comparisons test on log10-transformed
867 values and are indicated in the graphs (*, P < 0.005, **, P < 0.01, ***, P < 0.001, ****, P < 0.0001).

868 **Fig. 5: Consensus and PHOT-specific GRNs indicate extensive co-regulation of CCM and photoprotective**
869 **genes.** Top: Venn diagram depicting the overlap of the top 10 predicted TFs of the curated CCM and
870 photoprotective (PhPr) genes based on **a.** the consensus or **c.** PHOT-specific GRN. Bottom: Network
871 representation of the top ten TF sets of **b.** the consensus network or **d.** the PHOT-specific GRN (center nodes,
872 same color code as in panel **a**) and the target genes used for prediction (left and right columns of nodes,
873 photoprotection genes are shown in green, qE-related genes in blue, and CCM genes in red. In **b** the plotted
874 regulatory strength corresponds to $log(\frac{1}{r_{consen}})$, in **d**., it corresponds the GENIE3 edge weights denoting
875 random forest importance measure. The edge width is proportional to the strength of the specific regulatory
876 interaction. Size of the TF nodes corresponds to the sum of all plotted target gene edge weights.

877

878

879

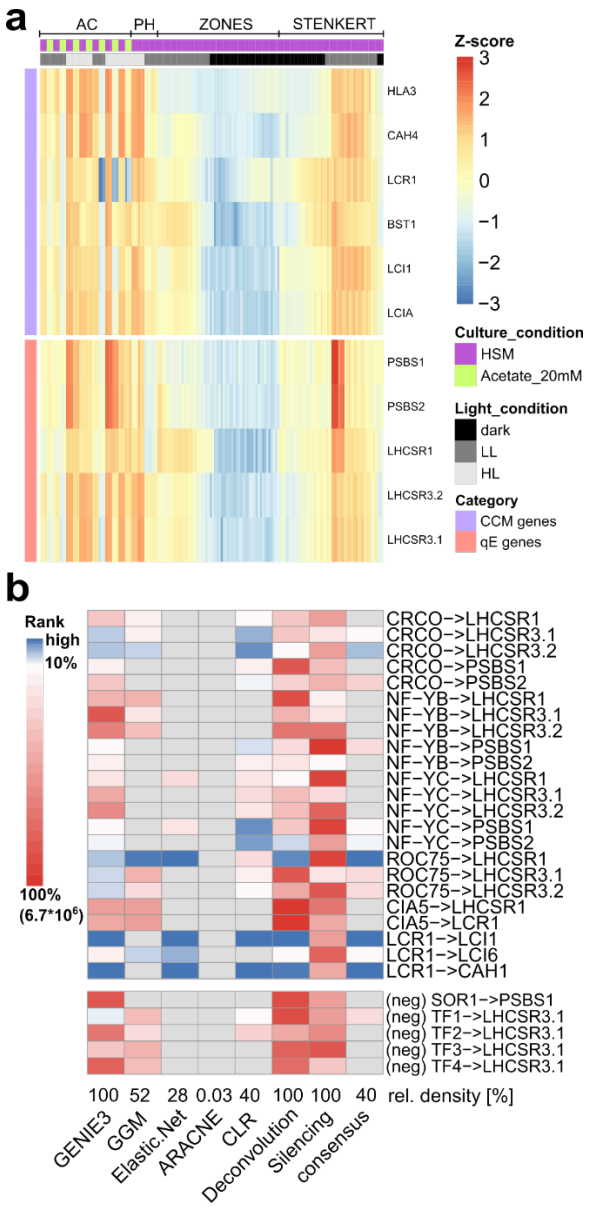

Fig. 1: Characterization of the consensus GRN inferred by employing a compendium of RNA-seq data from diverse light and culture conditions. **a.** Expression levels of representative CCM and qE genes are plotted over all samples used for network inference (z-scaled log values are depicted). The column annotation gives information on the culture conditions and data set (see also **Supplementary Table 1**); no clustering was applied. **Supplementary Fig. 1** shows an enlarged version of this figure with sample names included. **b.** The heatmap rows correspond to experimentally validated or invalidated (neg) gene regulatory interactions involved in qE and CCM, curated from literature. The heatmap indicates ranking of these interactions by different approaches and the consensus network. Edges are considered highly ranked (depicted in blue) if they are above the 10% network density threshold. Edges ranked below this threshold are depicted in red. Edges that were not included in the given network are marked in grey. At the bottom of the heatmap the relative number of edges inferred by each approach is provided. ARACNE and Silencing columns were only plotted for comparison and were not used in building the consensus GRN (see Methods). TF1: MYB-like DNA-binding protein, Cre01.g034350; TF2: RWP8, RWP-RK transcription factor, Cre04.g218050; TF3: RWP5, RWP-RK transcription factor, Cre06.g285600; TF4: bHLH domain-containing protein, Cre07.g349152)

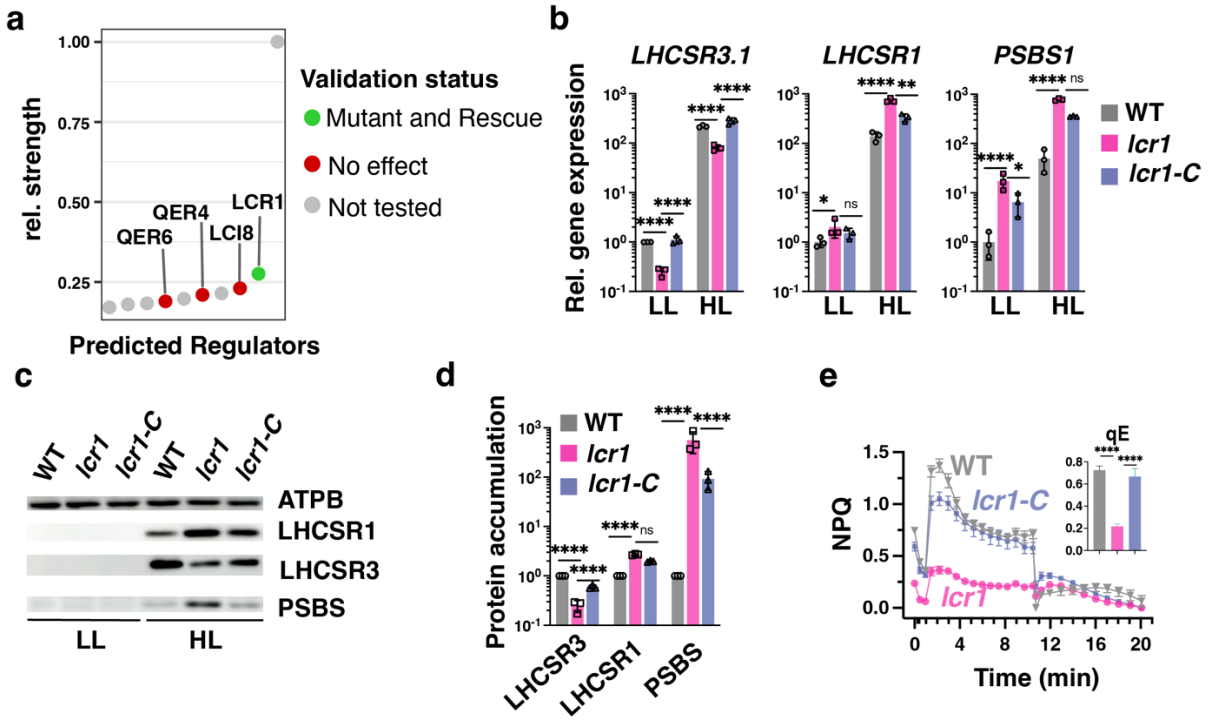

Fig. 2: Consensus GRN for light and acetate responses pinpoints LCR1 as regulator of qE-related genes. a. Dot plot of the relative regulatory strength of the top 10 regulators of qE-related genes in the consensus GRN (see Methods). TFs are marked in green if qE transcript levels were affected in the respective knock-out strain and this effect was reversed by complementation with the missing gene. TFs for which no effect was observed are marked in red. TFs for which no mutant lines were available are plotted in grey. **b.** WT, *lcr1* and *lcr1-C* cells were acclimated for 16h in LL (15 µmol photons m^{-2} s^{-1}). After sampling for the LL conditions, light intensity was increased to 300 µmol photons m^{-2} s^{-1} (HL); samples were taken 1 h (RNA) or 4 h (protein and photosynthetic measurements) after exposure to HL. Shown are relative expression levels of qE-related genes at the indicated conditions normalized to WT LL (*n* = 3 biological samples, mean ± sd). **c**. Immunoblot analyses of LHCSR1, LHCSR3, PSBS and ATPB (loading control) of one of the three biological replicates, under the indicated conditions. **d.** Quantification of immunoblot data of all replicates in panel **c** after normalization to ATPB. Shown are the HL treated samples; WT protein levels were set as 1. **e.** NPQ and calculated qE (as an inset) 4h after exposure to HL (*n* = 3 biological samples, mean ± s.d). The p-values for the comparisons are based on ANOVA Dunnett's multiple comparisons test and as indicated in the graphs (*, P < 0.005, **, P < 0.01, ***, P < 0.001, ****, P < 0.0001). Statistical analyses for panels **b** and **d** were applied on log10-transformed values.

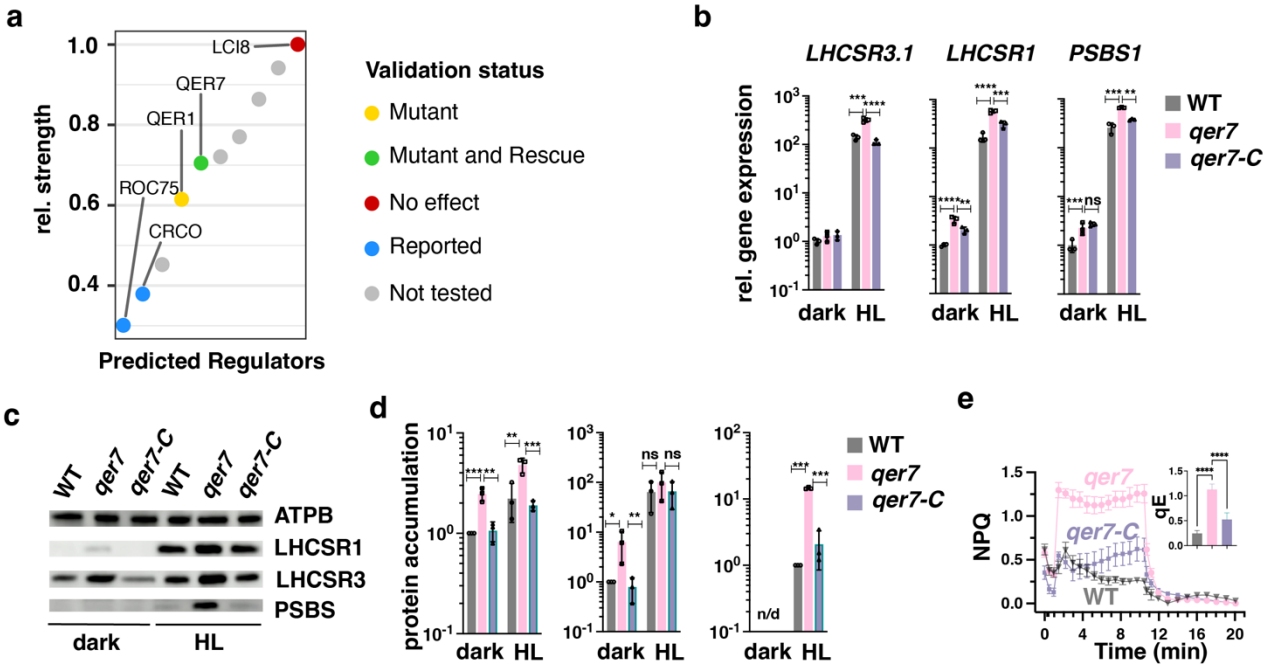

Fig. 3: A PHOT-specific GRN pinpoints QER7 as a suppressor of the expression of qE-related genes. a. Dot plot of the relative regulatory strength of the top 10 regulators of qE-related genes in the PHOT-specific GRN (see **Methods**). TFs are marked in green if qE transcript levels were affected in the respective knock-out strain and this effect was reversed by complementation with the knocked-out gene, in yellow, if the effect was not reversed by complementation, and in red, if no mutant effect was observed in the mutant. TFs for which no mutant lines were available are plotted in grey. **b**. WT, *qer7* and *qer7-C* cells were synchronized under 12h light (15 µmol m^{-2} s^{-1})/12h dark cycles. After sampling for the dark conditions (end of the dark phase), cells were exposed to 300 µmol photons m^{-2} s^{-1} (HL); samples were taken 1 h (RNA) or 4 h (protein and photosynthetic measurements) after exposure to HL. Shown are relative expression levels of qE-related genes at the indicated conditions normalized to WT LL (*n* = 3 biological samples, mean ± sd). **c**. Immunoblot analyses of LHCSR1, LHCSR3 and ATPB (loading control) of one of the three biological replicate set of samples, under the indicated conditions. **d.** Quantification of immunoblot data of all replicates in panel **c** after normalization to ATPB. WT protein levels at HL were set as 1. **e.** NPQ and qE, measured 4h after exposure to HL (*n* = 3 biological samples, mean ± sd). The p-values for the comparisons are based on ANOVA Dunnett's multiple comparisons test and are indicated in the graphs (*, P < 0.005, **, P < 0.01, ***, P < 0.001, ****, P < 0.0001). Statistical analyses for panel **b** and **d** were applied on log10- transformed values.

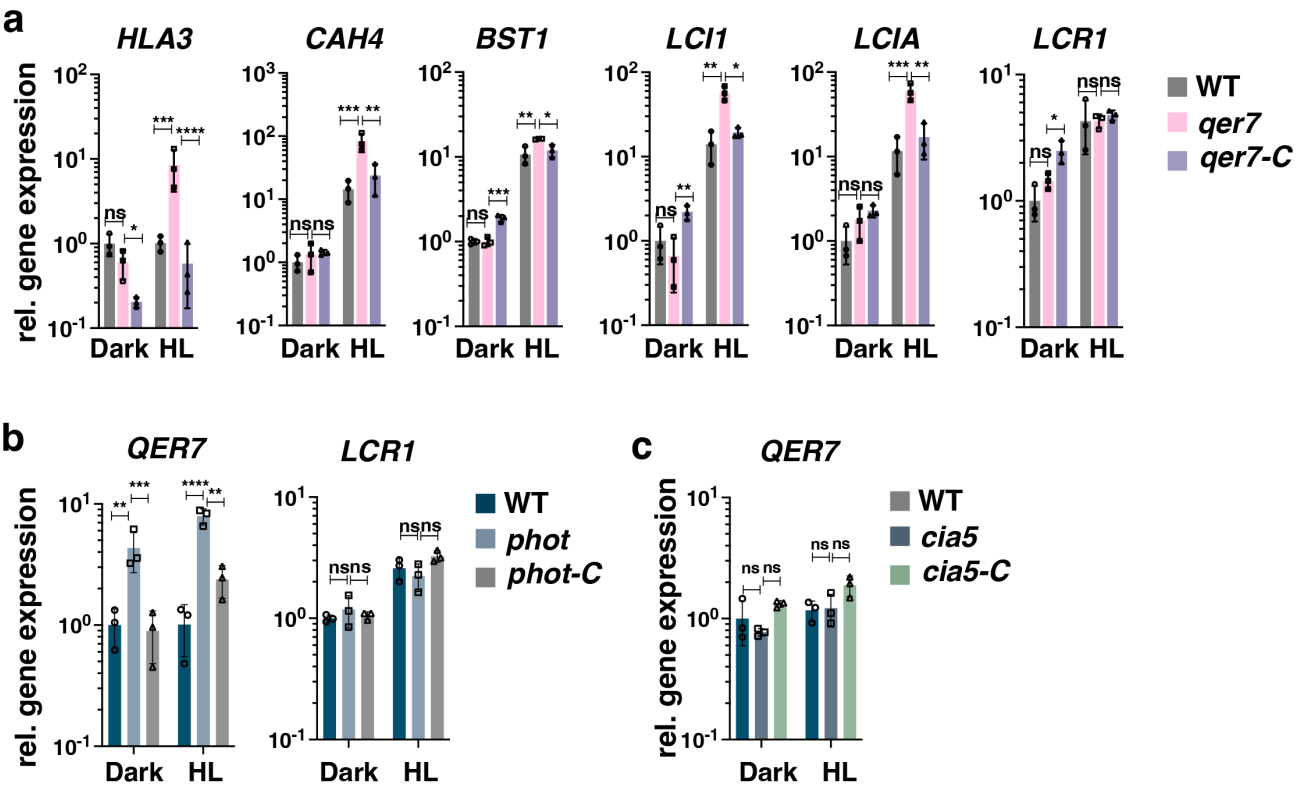

935

936 **Fig. 4: QER7 suppresses transcription of CCM genes and depends on PHOT.** *qer7*, *phot* and *cia5* cells alongside
937 with their complemented lines (*qer7-C*, *phot-C* and *cia5-C* respectively*) and* WT backgrounds, were
938 synchronized under 12h light (15 µmol m^{-2} s^{-1})/12h dark cycles, in photoautotrophic conditions (Sueoka's high
939 salt medium; HSM), at 23 °C in Erlenmeyer flasks shaken at 125 rpm. After sampling at the end of the dark
940 phase, cells were exposed to 300 µmol photons m^{-2} s^{-1} (HL) and samples were taken 1 h after HL exposure. **a.**
941 Relative expression levels of CCM genes at the indicated conditions. **b** Relative expression levels of *QER7* and
942 *LCR1* in WT, *phot* and *phot-C*. **c** Relative expression levels of *QER7* in WT, *cia5* and *cia5-C.* In all cases (**a**, **b** and
943 **c**) expression levels were normalized to WT LL (*n* = 3 biological samples, mean ± sd). The p-values for the
944 comparisons are based on ANOVA employing Dunnett's multiple comparisons test on log10-transformed
945 values and are indicated in the graphs (*, P < 0.005, **, P < 0.01, ***, P < 0.001, ****, P < 0.0001).

946

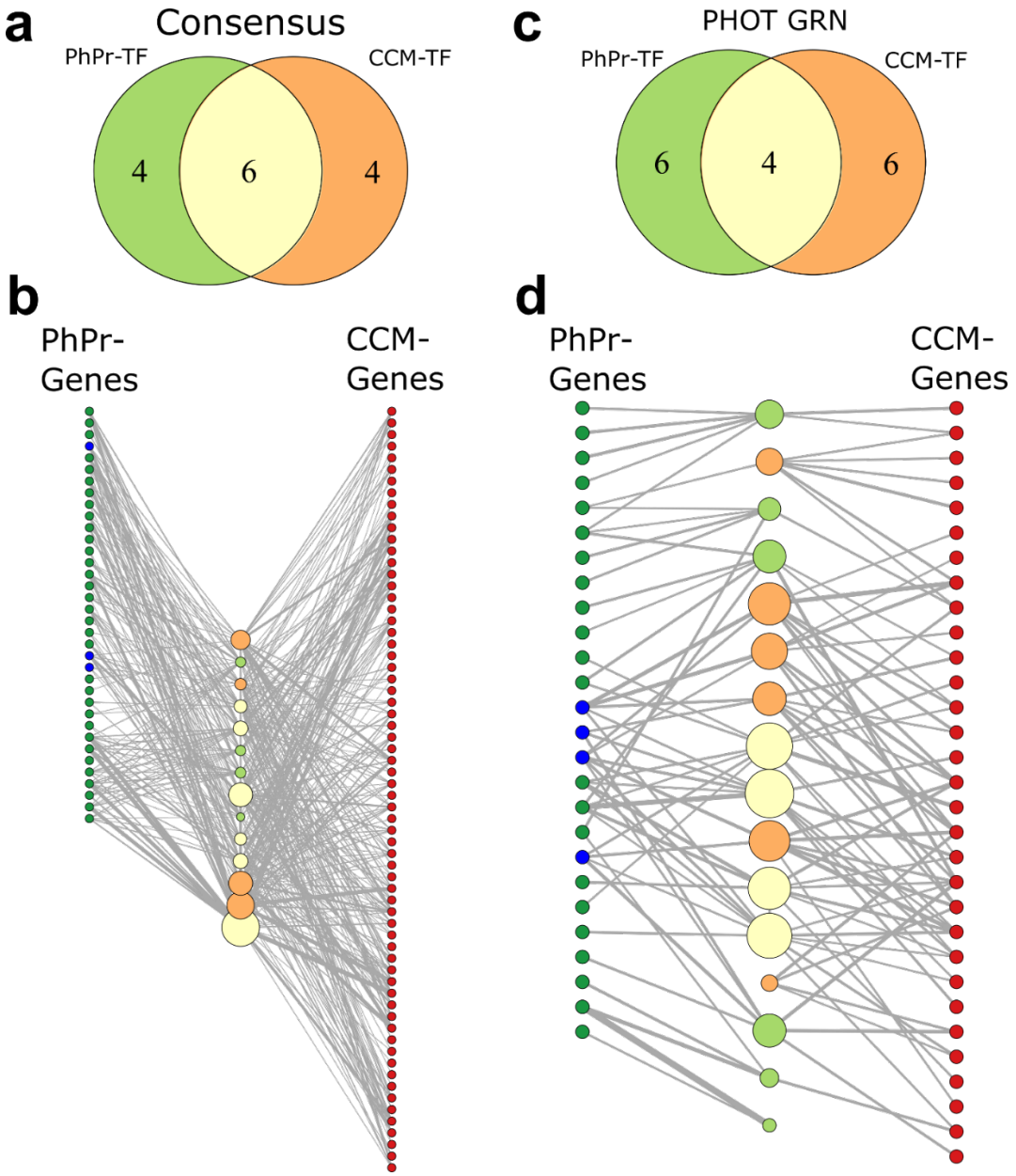

Fig. 5: Consensus and PHOT-specific GRNs indicate extensive co-regulation of CCM and photoprotective genes. Top: Venn diagram depicting the overlap of the top 10 predicted TFs of the curated CCM and photoprotective (PhPr) genes based on **a.** the consensus or **c.** PHOT-specific GRN. Bottom: Network representation of the top ten TF sets of **b.** the consensus network or **d.** the PHOT-specific GRN (center nodes, same color code as in panel **a**) and the target genes used for prediction (left and right columns of nodes, photoprotection genes are shown in green, qE-related genes in blue, and CCM genes in red. In **b** the plotted regulatory strength corresponds to $log(\frac{1}{r_{consen}})$, in **d**., it corresponds the GENIE3 edge weights denoting random forest importance measure. The edge width is proportional to the strength of the specific regulatory interaction. Size of the TF nodes corresponds to the sum of all plotted target gene edge weights.

Supplementary Materials for

Widening the landscape of transcriptional regulation of green algal photoprotection

Authors

Marius Arend[†], Yizhong Yuan[†], M. Águila Ruiz-Sola, Nooshin Omranian, Zoran Nikoloski[*], Dimitris Petroutsos[*]

[*]Corresponding Authors. nikoloski@mpimp-golm.mpg.de (Z.N.), dimitris.petroutsos@cea.fr (D.P.)

This PDF file includes:

Supplementary Notes 1 and 2

Supplementary Figs. 1 to 15

Other Supplementary Materials for this manuscript include the following:

Supplementary Tables 1 to 13 (to be downloaded as a single excel file)

29 **Supplementary Note 1**

30 In the course of independent projects aiming to identify novel regulators of *LHCSR3*, we have investigated the
31 role of four transcriptional factors, designated as TF1-4, in regulating expression of *LHCSR3.1* (*TF1*: MYB-like
32 DNA-binding protein, Cre01.g034350; *TF2*: RWP8, RWP-RK transcription factor, Cre04.g218050; *TF3*: RWP5,
33 RWP-RK transcription factor, Cre06.g285600; *TF4*: bHLH domain-containing protein, Cre07.g349152).
34 Mutants bearing mutations in TF1-4 genes were ordered from the CliP library [1]. After confirming
35 (Supplementary Fig. 2a) that expression of the genes of interest was abolished (*tf1-3* mutants) or was
36 significantly higher than in WT (for the case of *tf4-oe*), we applied the following experimental setup to probe
37 for *LHCSR3.1* expression: WT and mutant cells were acclimated for 16h in LL (15 µmol photons m^{-2} s^{-1}). After
38 sampling under the LL condition, light intensity was increased to 300 µmol photons m^{-2} s^{-1} (HL); samples for
39 RNA extraction were taken after 1 h of exposure to HL. Our data showed that WT and mutants had similar
40 expression levels of *LHCSR3.1* (**Supplementary Fig. 2**), excluding a role of these TFs in regulating transcription
41 of *LHCSR3.1*.

42 **Supplementary Note 2**

43 Simulation studies[2] indicated that the top 10% of the edges in the consensus network are enriched in positive
44 interactions if the underlying approaches perform better than guessing. Thus, a higher overlap with the
45 consensus networks is expected to result in improved predictions. We found that the interactions from the
46 network deconvolution approach exhibited the largest overlap with the consensus network, while GGM
47 assigns the highest rank to consensus interactions (**Supplementary Fig. 4a**). Repeating this analysis by
48 including the two worse performing approaches (i.e. ARACNE and Silencing) resulted in no qualitative changes
49 in the overlap (**Supplementary Fig. 4b**) and only 7.47% of difference in the included interactions compared to
50 the original consensus network, demonstrating the robustness of the inferred interactions. Considering the
51 10% network density threshold, we also inspected the proportion of TF-TF interactions in the different
52 networks and their consensus; we found that it ranges from 2.55% in the GENIE3 network to 2.77% in the
53 network deconvolution approach (**Supplementary Fig. 4c**). Since the fully connected network, containing all
54 possible TF-TF and TF-target interactions, has a relative TF-TF interaction content of 2.52%, these findings
55 suggest an enrichment of TF-TF interactions in GRNs inferred by all five approaches considered in the
56 consensus.

57 **Supplementary list of references**

58 1. Li, X. *et al.* A genome-wide algal mutant library and functional screen identifies genes required for eukaryotic
59 photosynthesis. *Nat. Genet.* **51,** 627–635 (2019).
60 2. Marbach, D. *et al.* Wisdom of crowds for robust gene network inference. *Nat. Methods* **9,** 796–804 (2012).

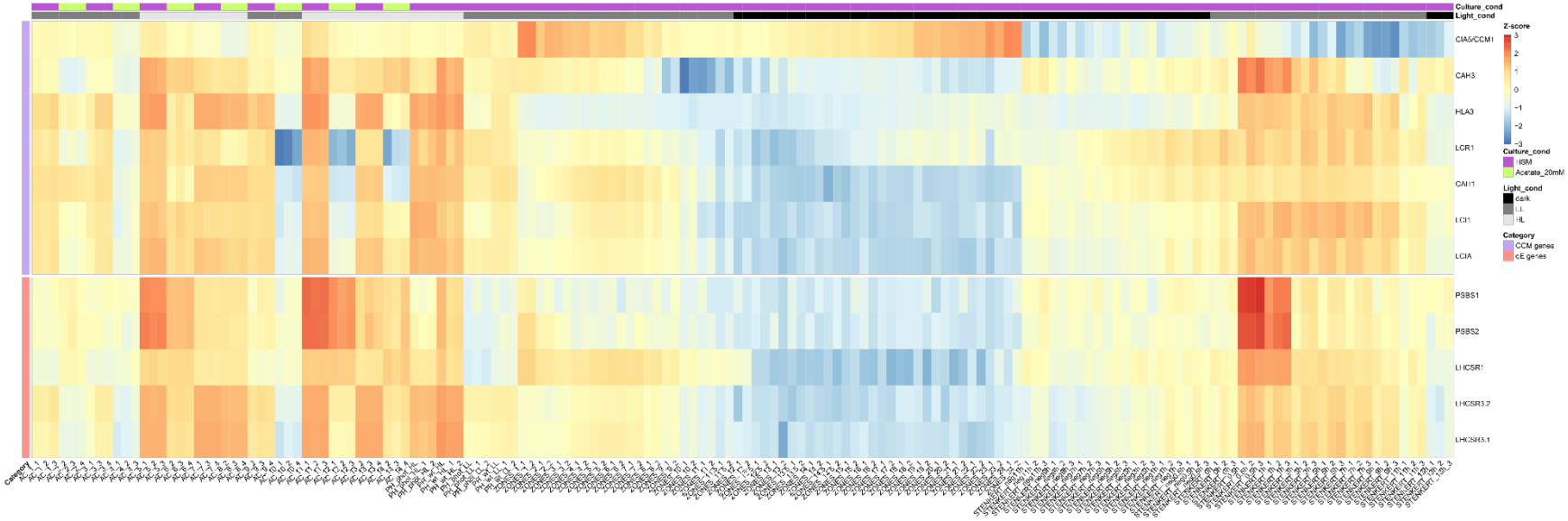

Supplementary Fig. 1: Z-score of log-transcript levels for representative CCM and qE genesin the used RNAseq data set. Enlarged representation of **Fig. 1a** with sample names included (see **Supplementary Table 1** for more details). The last digit of the column names indicates the replicate number. The column annotation provides information on the culture conditions. No clustering was applied.

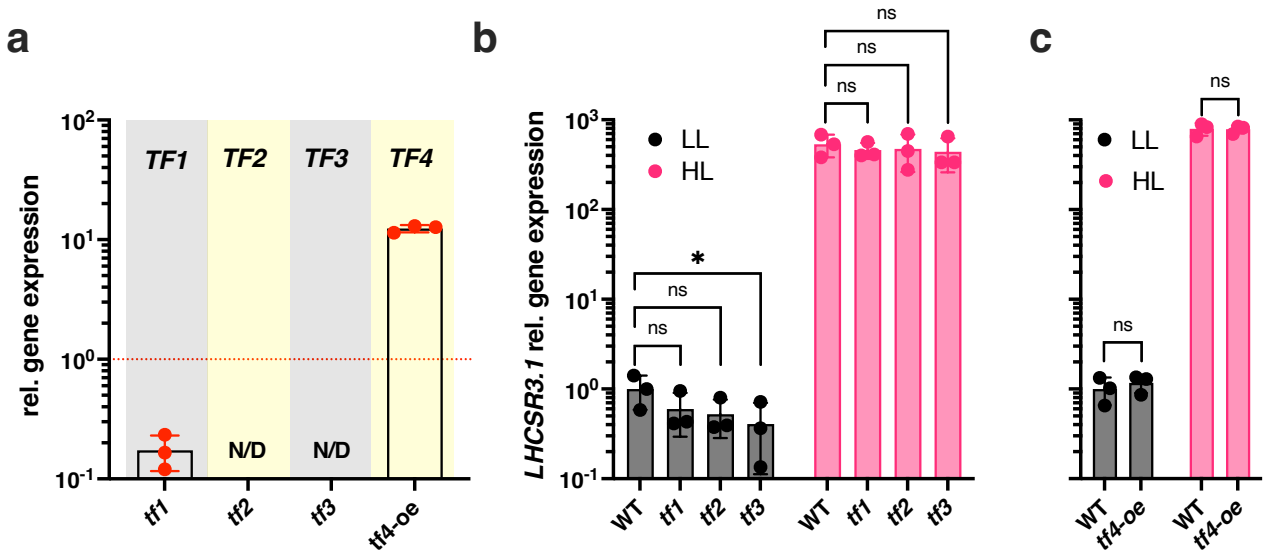

Supplementary Fig. 2: *LHCSR3.1* expression in mutants bearing mutations in transcription factors TF1-4. a Relative expression levels of *TF1-4 in tf1, tf2, tf3* and *tf4* mutant strains, grown under LL conditions in tris-acetate-phosphate (TAP) medium, normalized to WT (indicated as a red dashed line in the figure); N/D: non-detectable. **b** and **c** WT, *tf1, tf2, tf3 and tf4* cells were acclimated for 16h in LL (15 µmol photons m^{-2} s^{-1}). After sampling under the LL conditions, light intensity was increased to 300 µmol photons m^{-2} s^{-1} (HL); samples were taken 1 h after exposure to HL. Shown are relative expression levels of *LHCSR3.1* at the indicated conditions normalized to WT LL (*n* = 3 biological samples, mean ± sd) for **b** WT (CC-4533) and tf1-3 and **c** for WT (CC-125) and tf4-oe, a strain overexpressing *tf4* in the CC-125 background. The p-values for the comparisons between the mutants and the WT are based on ANOVA Dunnett's multiple comparisons test using log10- transformed values; the p-values are indicated in the graphs (*, $P < 0.005$; ns: non-significant). *TF1*: MYB-like DNA-binding protein, Cre01.g034350; *TF2*: RWP8, RWP-RK transcription factor, Cre04.g218050; *TF3*: RWP5, RWP-RK transcription factor, Cre06.g285600; *TF4*: bHLH domain-containing protein, Cre07.g349152).

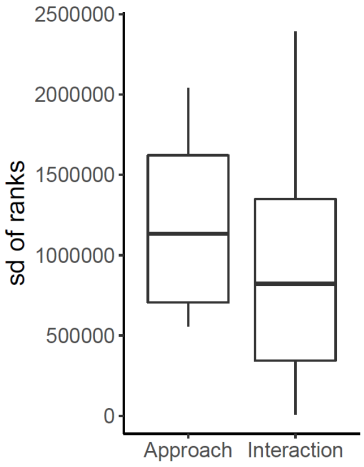

Supplementary Fig. 3: Variation in ranks of known interactions across approaches and interactions from different inference approaches. Boxplots of the standard deviation of ranks calculated for the curated interactions plotted in **Fig. 1b** over all ranks assigned by one approach or over all ranks assigned to one interaction.

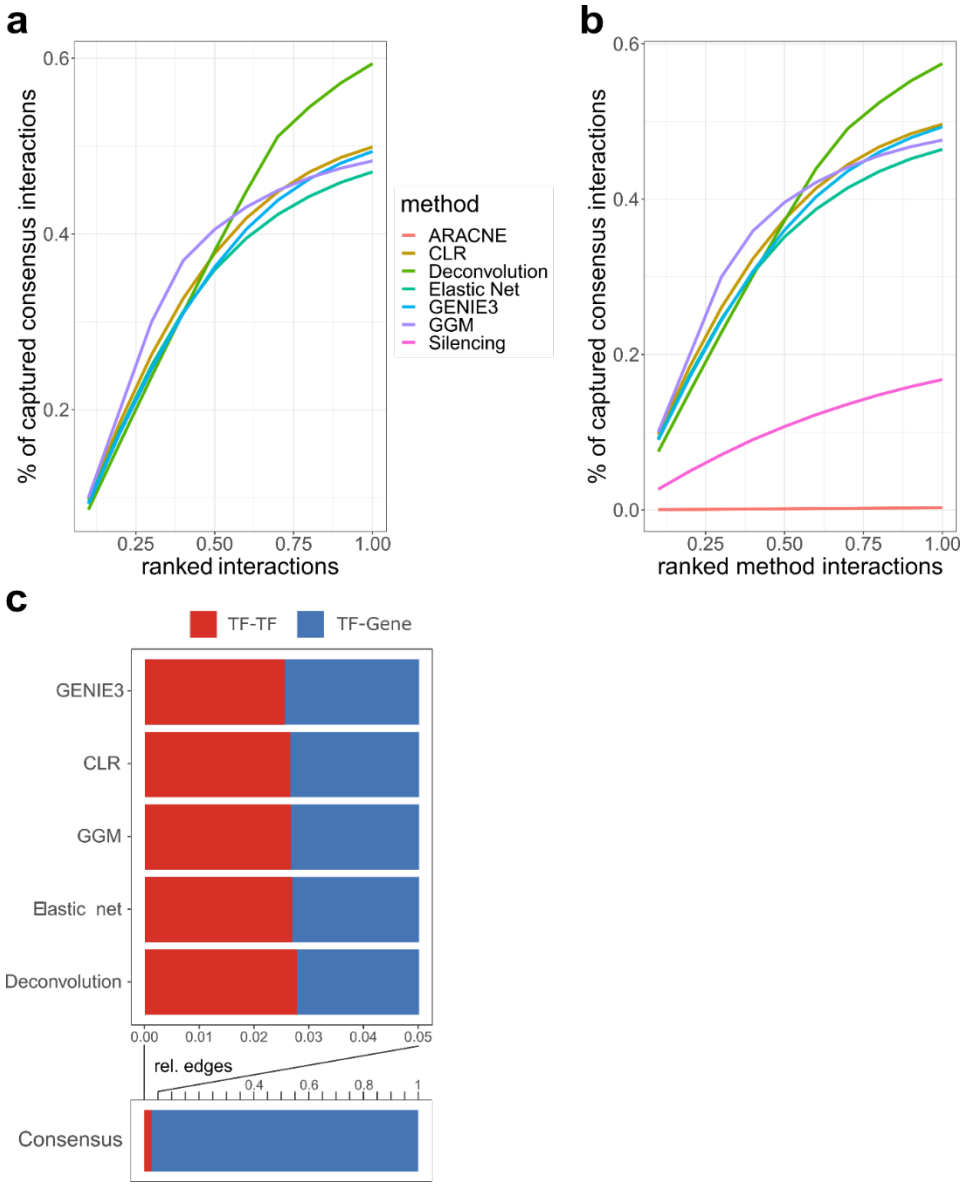

Supplementary Fig. 4: Overlap of consensus network with individual inference methods and proportion of TF-TF interactions in the obtained GRNs. a. The graph shows the overlap between the edges of the consensus network and the ranked interactions of the individual approaches normalized to the total number of edges in the consensus network used for regulator prediction. **b.** Same as in a but plotting the overlap with a consensus of all used approaches (including ARACNE and Silencing). **c**. Bar plots provide the proportion of TF-TF interactions in comparison to TF-target gene interactions contained in the GRNs inferred by the different approaches and the consensus GRN resulting from their integration. All depicted analyses considered only the interactions within in the 10% network density threshold (see **Methods**).

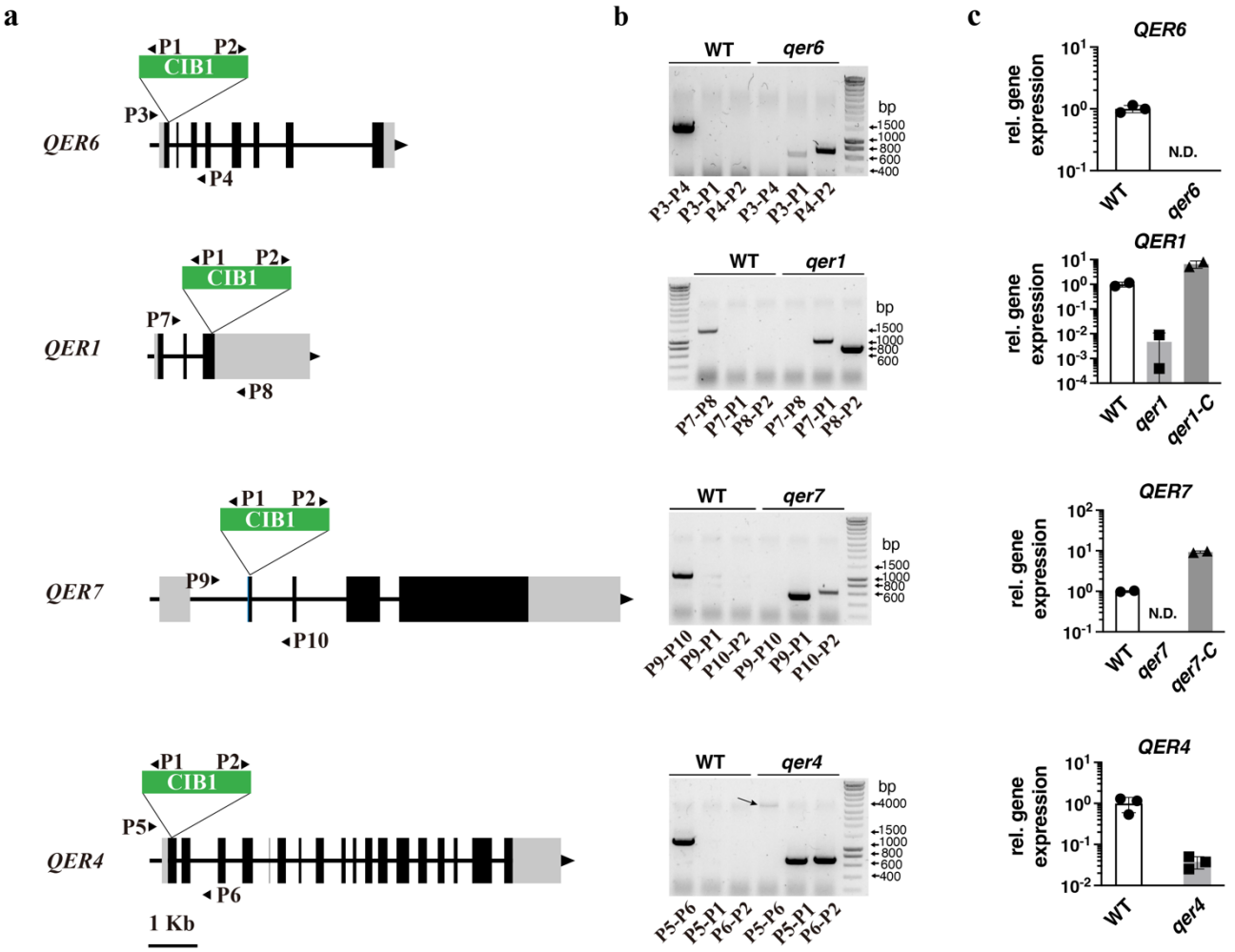

Supplementary Fig. 5: Genotyping of CLiP mutants affected in the predicted regulators of qE-related genes. **a**. Insertion map of the CIB1 cassette in the different genes. Exons are shown in black, introns as interconnecting lines, 5'UTR and 3'UTR in light gray, and primers in arrows. The insertion site of the CIB1 cassette is indicated by the triangle; **b**. PCR-validation of the insertion site in the different CLiP mutants using genomic DNA. To confirm the CIB1 insertion site, gene-specific primers were used that anneal upstream and downstream of the predicted insertion site of the cassette (primer pairs P3-P4, P7-P8, P9-P10 and P5-P6 for *qer6*, *qer1*, *qer7* and *qer4* respectively*;* **Supplementary Table 12**). Pairs of primers used are indicated at the bottom of the agarose gels used to separate the PCR products. Note that the PCR product of P5-P6 is indicated by an arrow. **c.** Relative expression levels of predicted qE regulator genes in the different CLiP mutants after exposure to HL (300 µmol photons m^{-2} s^{-1}) for 1h.

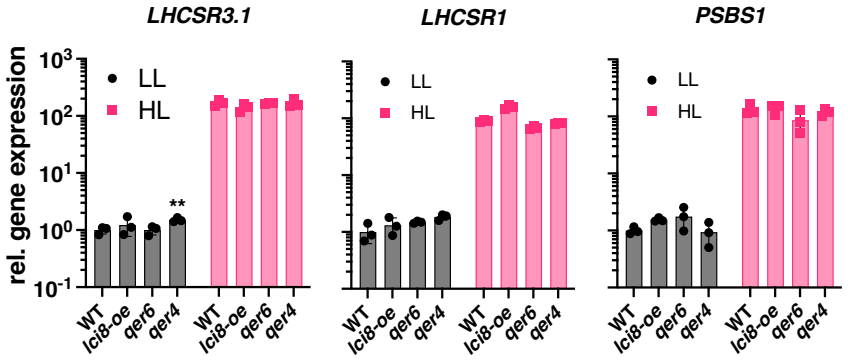

Supplementary Fig. 6: qE gene and protein expression in mutants bearing mutations in predicted qE regulator genes. WT, *lci8-oe, qer6* and *qer4* cells were acclimated for 16h in LL (15 µmol photons m^{-2} s^{-1}). After sampling for the LL conditions, light intensity was increased to 300 µmol photons m^{-2} s^{-1} (HL); samples were taken 1 h after exposure to HL. Shown are relative expression levels of *LHCSR3.1*, *LHCSR1* and *PSBS1* at the indicated conditions normalized to WT LL (*n* = 3 biological samples, mean ± sd). The p-values for the comparisons between the mutants and the WT are based on ANOVA Dunnett's multiple comparisons test on log10- transformed values and are indicated in the graphs (**, P < 0.01).

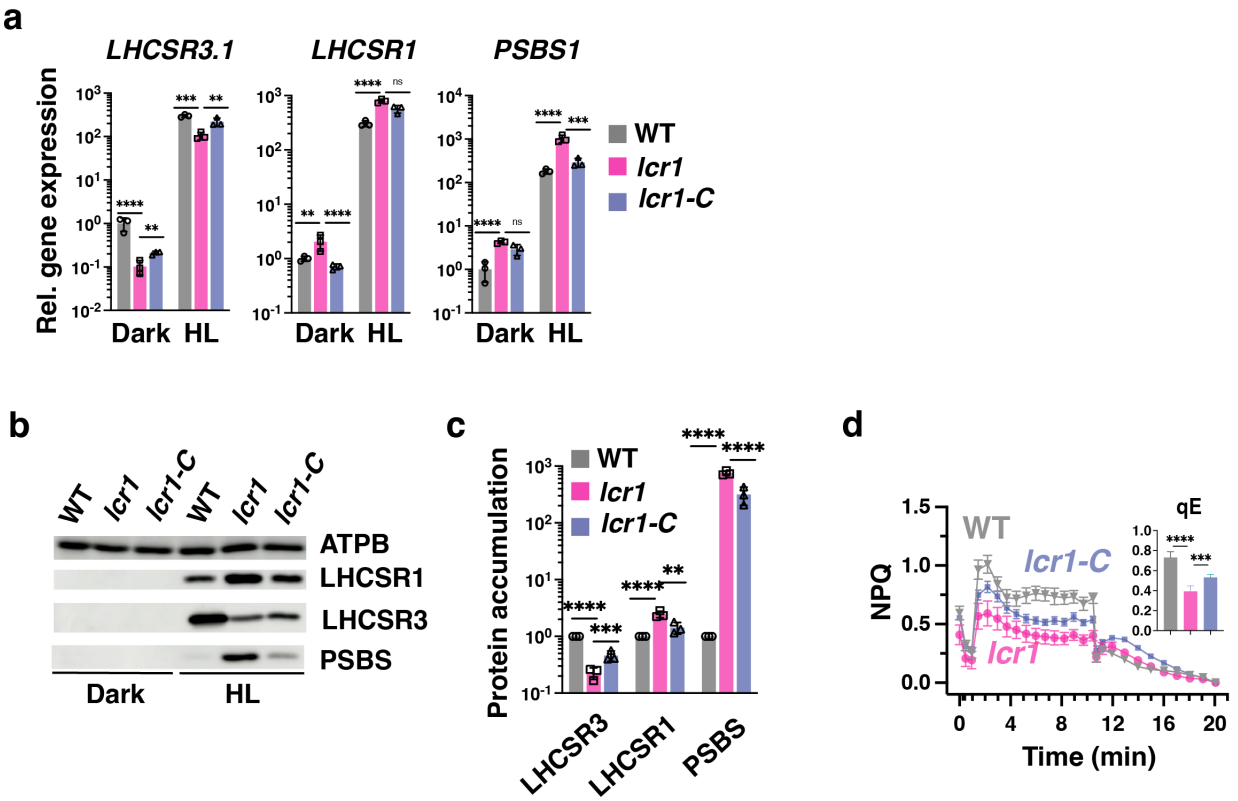

Supplementary Fig. 7: LCR1 is required for proper expression of qE-related genes during transitions from dark-to-light. WT, *lcr1* and *lcr1-C* cells were acclimated for 16h in darkness. After sampling for the dark conditions, light intensity was increased to 300 µmol photons m^{-2} s^{-1} (HL); samples were taken 1 h (RNA) or 4 h (protein and photosynthetic measurements) after exposure to HL. **a**. Relative expression levels of qE genes at the indicated conditions normalized to WT LL (*n* = 3 biological samples, mean ± sd). **b**. Immunoblot analyses of LHCSR1, LHCSR3, PSBS and ATPB (loading control) of one out of the three biological replicate samples, under the indicated conditions. **c.** Summary graph of immunoblots of all replicate samples of Supplementary Fig. 4b after normalization to ATPB. Shown are the HL treated samples; WT protein levels were set as 1. **d.** NPQ and calculated qE, 4h after exposure to HL (*n* = 3 biological samples, mean ± s.d). The p-values for the comparisons are based on ANOVA Dunnett's multiple comparisons test and are indicated in the graphs (*, P < 0.005, **, P < 0.01, ***, P < 0.001, ****, P < 0.0001). Statistical analyses for panel **a** and **c** were applied on log10- transformed values.

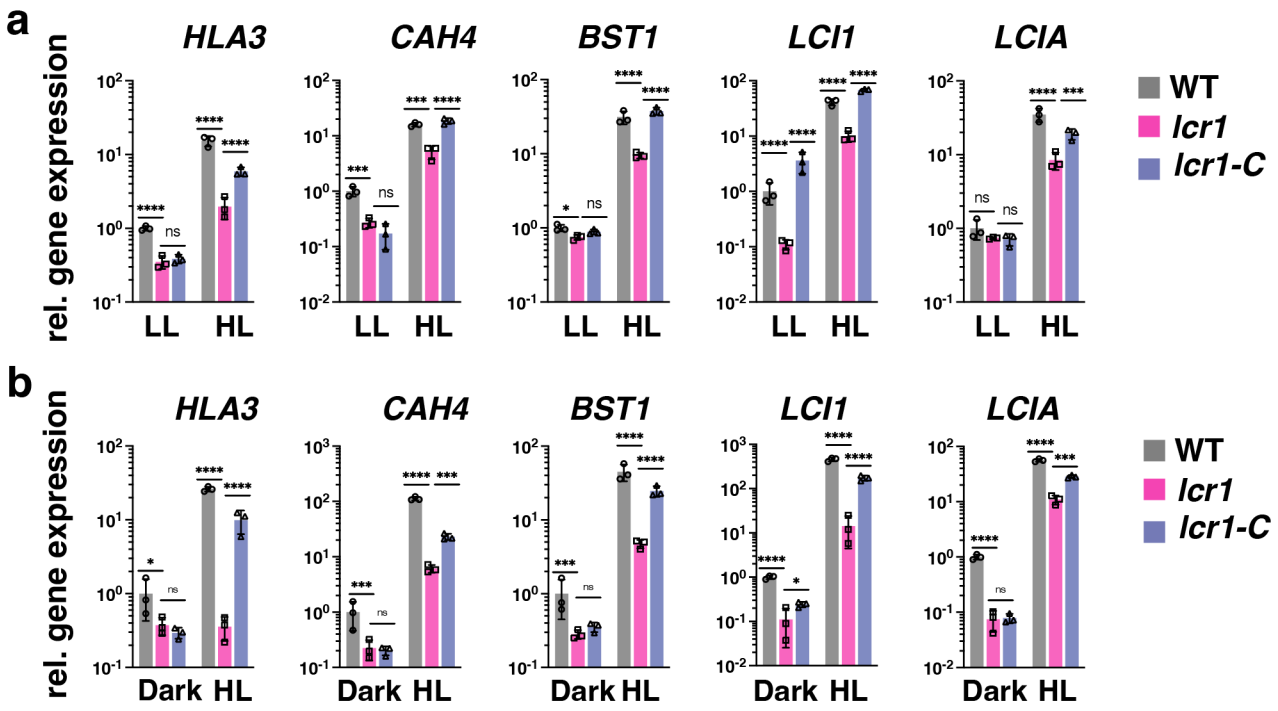

Supplementary Fig. 8: LCR1 activates the transcription of CCM genes in LL and dark-acclimated cells. a. WT, *lcr1* and *lcr1-C* cells were acclimated for 16h in LL (15 µmol photons m^{-2} s^{-1}). After sampling under LL conditions, light intensity was increased to 300 µmol photons m^{-2} s^{-1} (HL) and samples were taken 1 h after exposure to HL. Relative expression of CCM genes at the indicated conditions normalized to WT under LL. **b**. Relative expression of CCM genes acclimated in 16h of darkness (*n* = 3 biological samples, mean ± sd). The p-values for the comparisons are based on ANOVA Dunnett's multiple comparisons test on log10- transformed values and are indicated in the graphs (*, P < 0.005, **, P < 0.01, ***, P < 0.001, ****, P < 0.0001).

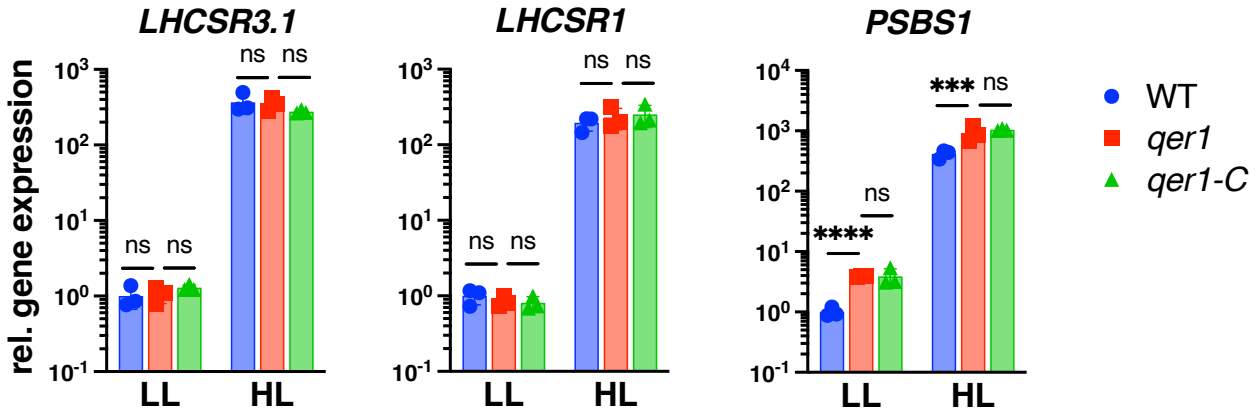

Supplementary Fig.9: Complementation of *qer1* with *QER1* (*qer1-C* strain) fails to rescue the *LHCSR1* and *PSBS* phenotypes. WT, *qer1* and *qer1-C* cells were acclimated for 16h in LL (15 µmol photons m^{-2} s^{-1}). After sampling for the dark conditions, light intensity was increased to 300 µmol photons m^{-2} s^{-1} (HL); RNA samples were taken 1 h after exposure to HL. Shown are relative expression levels of qE genes at the indicated conditions normalized to WT LL (*n* = 3 biological samples, mean ± sd). The p-values for the comparisons are based on ANOVA Dunnett's multiple comparisons test on log10- transformed values and are indicated in the graphs (*, P < 0.005, **, P < 0.01, ***, P < 0.001, ****, P < 0.0001).

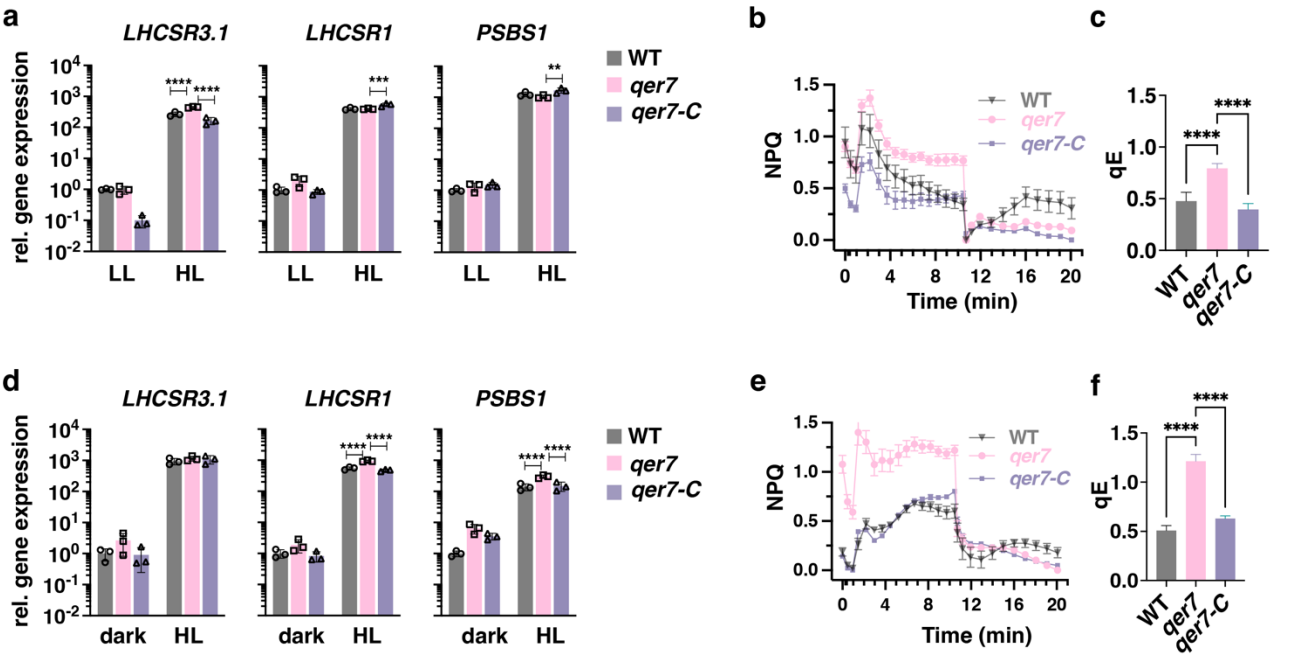

Supplementary Fig.10: Relative expression of qE-related genes in asynchronous *qer7* cells. WT, *qer7* and *qer7-C* cells were acclimated for 16h in LL (15 µmol photons m^{-2} s^{-1}; **a-c**) or darkness (**d-f**). After sampling for the LL or dark conditions, light intensity was increased to 300 µmol photons m^{-2} s^{-1} (HL) and samples were taken 1 h (RNA) or 4 h (photosynthetic measurements) after exposure to HL. **a, d**. Relative expression of qE and CCM genes at the indicated conditions normalized to WT LL (**a**) or dark (**d**) respectively (*n* = 3 biological samples, mean ± sd). **b, e.** NPQ and **c, f.** calculated qE, 4h after exposure to HL (*n* = 3 biological samples, mean ± s.d. The p-values for the comparisons are based on ANOVA Dunnett's multiple comparisons test and are indicated in the graphs (*, P < 0.005, **, P < 0.01, ***, P < 0.001, ****, P < 0.0001). Statistical analyses for panel **a** and **d** were applied on log_{10}- transformed values.

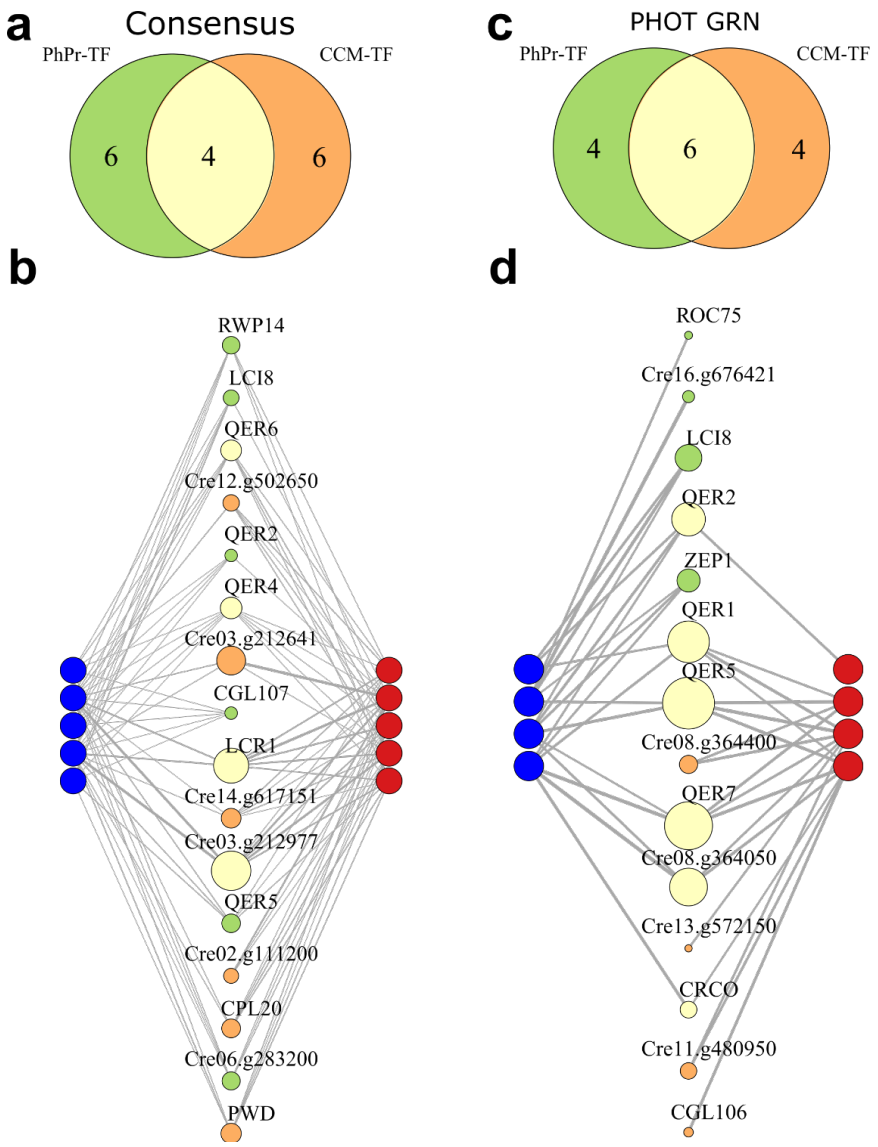

Supplementary Fig. 11: Reconstructed GRNs capture experimentally found regulators of qE and CCM. Top: Venn diagram depicting the overlap of the top 10 predicted regulators of CCM genes included in **Fig. 4a ,** and qE genes based on **a.** the consensus or **c.** PHOT-specific GRN. Bottom: Network representation of the top ten TF sets of **b.** the consensus network or **d.** the phot GRN (center nodes, same color code as in panel **a**) and the target genes present in the respective network. qE-related genes (*LHCSR1*, *LHCSR3.1*, *LHCSR3.2*, *PSBS1*, *PSBS2*) are plotted in blue, and CCM genes included in **Fig. 4a** (*HLA3, CAH4, LCR1, BST1, LCI1*, *LCIA*) in red. In **b** the plotted regulatory strength corresponds to $log(\frac{1}{r_{consen}})$, in **d**., it corresponds to the GENIE3 edge weights denoting random forest importance measure. The edge width is proportional to the strength of the specific regulatory interaction. Size of the TF nodes corresponds to the sum of all plotted target gene edge weights. See also **Supplementary Table 4,6** for QER locus IDs.

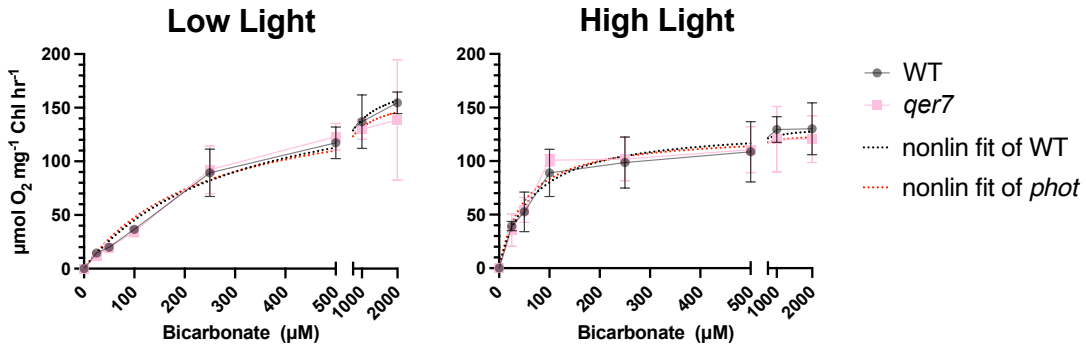

Supplementary Fig. 12: Ci affinity measurements in *qer7*. Oxygen evolution as a function of external Ci for WT and *qer7* cells grown under continuous LL (15 µmol m^{-2} s^{-1}) or exposed to HL (300 µmol m^{-2} s^{-1}) for 4h, in photoautotrophic conditions (Sueoka's high salt medium; HSM), at 23 °C in Erlenmeyer flasks shaken at 125 rpm. Non-linear curve fitting to the Michaelis-Menten equation is shown in dotted lines. $k_{1/2}$(Ci) and Vmax values are presented in **Supplementary Table 7**.

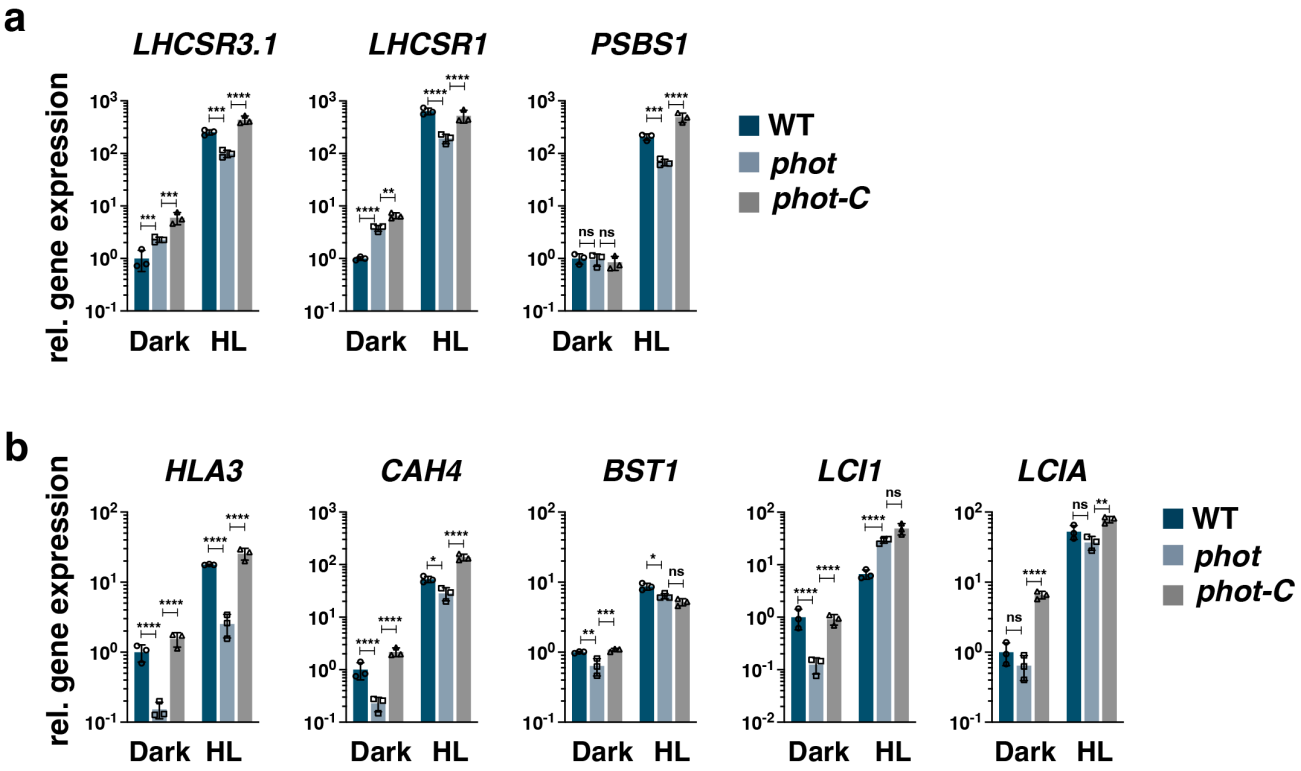

Supplementary Fig. 13: Phototropin dependent regulation of CCM gene expression. WT, *phot* and *phot-C* cells were synchronized under 12h light (15 µmol m^{-2} s^{-1})/12h dark cycles, in photoautotrophic conditions (Sueoka's high salt medium; HSM), at 23 °C in Erlenmeyer flasks shaken at 125 rpm. After sampling at the end of the dark phase, cells were exposed to 300 µmol photons m^{-2} s^{-1} (HL) and samples were taken 1 h after HL exposure. Relative expression levels of CCM (**a**) and qE (**b**) genes at the indicated conditions normalized to WT dark (n = 3 biological samples, mean ± sd). The p-values for the comparisons are based on ANOVA employing Dunnett's multiple comparisons test on log10-transformed values and are indicated in the graphs (*, $P < 0.005$, **, $P < 0.01$, ***, $P < 0.001$, ****, $P < 0.0001$).

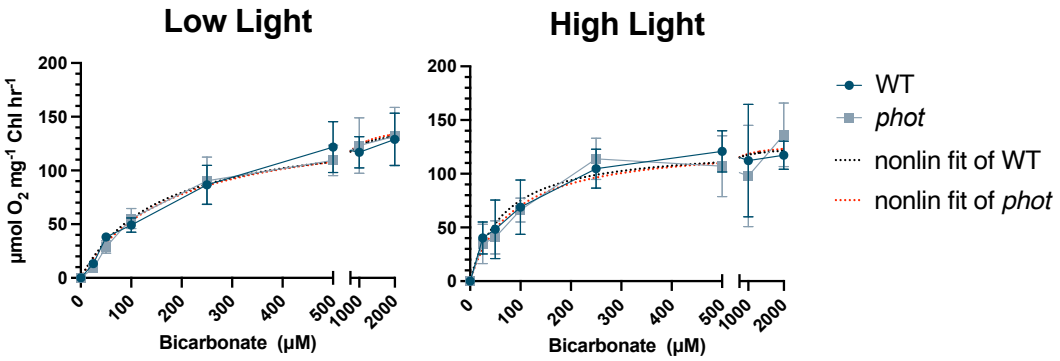

Supplementary Fig. 14: Oxygen evolution as a function of external Ci for WT and *phot* cells grown under continuous LL (15 µmol m^{-2} s^{-1}) or exposed to HL (300 µmol m^{-2} s^{-1}) for 4h, in photoautotrophic conditions (Sueoka's high salt medium; HSM), at 23 °C in Erlenmeyer flasks shaken at 125 rpm. Non-linear curve fitting to the Michaelis-Menten equation is shown in dotted lines. $k_{1/2}$(Ci) and Vmax values are presented in **Supplementary Table 7**.

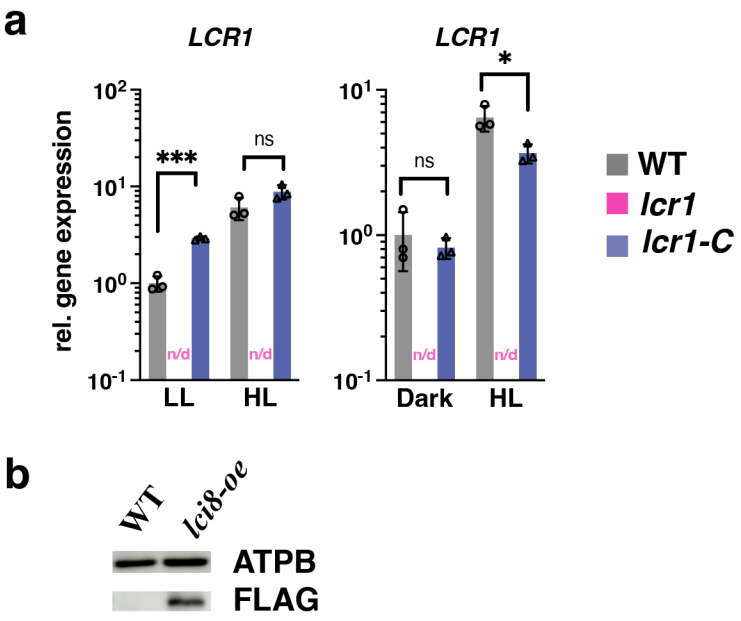

Supplementary Fig. 15: LCR1 mutation and LCI8 overexpression confirmation. a. Relative expression of *LCR1* in WT, *lcr1* and *lcr1-C* strains. Cells were acclimated for 16h in LL or darkness. After sampling for the LL or dark conditions, light intensity was increased to 300 µmol photons m^{-2} s^{-1} (HL), and samples for RNA purification were taken 1 h after exposure to HL (*n* = 3 biological samples, mean ± sd). *LCR1* gene expression was non-detectable (indicated as n/d in the graphs) in the *lcr1* mutant. **b.** Immunoblot analysis of LCI8-FLAG fused protein in WT and lci8-oe cells grown in TAP, LL. The p-values for the comparisons are based on unpaired t-tests on log10- transformed values and are indicated in the graphs (*, $P < 0.005$, ***, $P < 0.001$).

244 **Supplementary Table Captions**

245 **Supplementary Table 1**: RNAseq data sets used in this study.

246 **Supplementary Table 2:** List of Transcription factors used in this study; Family info was adapted from refs
247 41 and 42.
248
249 **Supplementary Table 3:** Edge list representation of the consensus network with mean ranks resulting from
250 Borda count election method (refs 48 and 52) as edge attributes.
251
252 **Supplementary Table 4:** Top 10 predicted regulators of qE genes in the consensus GRN.
253
254 **Supplementary Table 5**: Edge list representation of the PHOT-specific GRN with importance score from
255 GENIE 3 (ref. 68) as edge attributes.
256
257 **Supplementary Table 6:** Top 10 predicted regulators of qE genes in the PHOT-specific GRN.
258
259 **Supplementary Table 7:** Supplementary Table 7: $k_{1/2}$(Ci) and Vmax values calculated from External Data Fig.
260 12 and 14.
261
262 **Supplementary Table 8:** List of genes putatively involved in photoprotection used for regulator prediction.
263
264 **Supplementary Table 9:** List of genes putatively involved in CCM used for regulator prediction.
265
266 **Supplementary Table 10:** Global coregulators of photoprotection and CCM based on the consensus
267 network.
268
269 **Supplementary Table 11:** Global coregulators of photoprotection and CCM based on the PHOT specific
270 network.
271
272 **Supplementary Table 12:** PCR primers for CLiP mutant validation and complementation in this study.
273
274 **Supplementary Table 13**: RT-qPCR primers for all genes in this study.
275

276